frontiers | Frontiers in Energy Research

ORIGINAL RESEARCH
published: 14 July 2022
doi: 10.3389/fenrg.2022.873813

Metal Mobilization From CO_2 Storage Cap-Rocks: Experimental Reactions With Pure CO_2 or CO_2 SO_2 NO

J. K. Pearce[1,2]*, *G. W. Dawson*[2], *G. Southam*[2], *D. Paterson*[3], *D. Kirste*[4] *and S. D. Golding*[2]

[1]UQ Centre for Natural Gas, University of Queensland, Brisbane, QLD, Australia, [2]School of Earth and Environmental Sciences, University of Queensland, Brisbane, QLD, Australia, [3]Australian Synchrotron, ANSTO, Clayton, VIC, Australia, [4]Department of Earth Sciences, Simon Fraser University, Burnaby, BC, Canada

OPEN ACCESS

Edited by:
Maxim Lebedev,
Curtin University, Australia

Reviewed by:
Claire Nelson,
Columbia University, United States
Zhichao Yu,
Research Institute of Petroleum Exploration and Development (RIPED), China
Richard Woden,
University of Liverpool, United Kingdom

***Correspondence:**
J. K. Pearce
j.pearce2@uq.edu.au

Specialty section:
This article was submitted to Carbon Capture, Utilization and Storage, a section of the journal Frontiers in Energy Research

Received: *11 February 2022*
Accepted: *07 June 2022*
Published: *14 July 2022*

Citation:
Pearce JK, Dawson GW, Southam G, Paterson D, Kirste D and Golding SD (2022) Metal Mobilization From CO_2 Storage Cap-Rocks: Experimental Reactions With Pure CO_2 or CO_2 SO_2 NO. Front. Energy Res. 10:873813. doi: 10.3389/fenrg.2022.873813

CO_2 geological storage will be needed as part of the transition to lower greenhouse gas emissions. During CO_2 storage, the mobilization of metals from minerals to formation water *via* CO_2 water rock reactions may be a concern for water quality. The sources, behavior, and fate of metals, however, are not well understood. Metals in minerals of calcite cemented sandstone, feldspar-rich sandstone, and ironstone seal drill cores from a target storage site were characterized. The cores were reacted with low-salinity water and pure supercritical CO_2 or impure CO_2 with SO_2 and nitric oxide (NO), under reservoir conditions. Calcite cemented core underwent calcite dissolution with chlorite, plagioclase, and sulfide alteration. The highest concentrations of calcium and manganese were released in the reaction of calcite cemented sandstone seal, with the lowest mobilized arsenic concentration. Pure CO_2 reaction of the feldspar-rich sandstone seal resulted in calcite dissolution, with plagioclase, chlorite, kaolinite, illite, and sulfides corroded. Impure CO_2 reaction of the feldspar-rich sandstone led to additional corrosion of apatite, pyrite, and sphalerite cements. Generally, dissolved iron, lead, zinc, and arsenic were released and then re-precipitated in oxide minerals or adsorbed. Calcium, manganese, and strontium were released primarily from calcite cement dissolution. Plagioclase corrosion was a second source of dissolved strontium, and chlorite dissolution a second source of manganese. Although sulfides contained higher concentrations of metals, the higher reactivity of carbonates meant that the latter were the main sources contributing to dissolved metal concentrations. The mineral content of the seal cores, and the injected gas mixture, had an impact on the type and concentration of metals released. The ubiquitous presence of carbonate minerals means that this study is applicable to understanding the potential risk factors for water quality changes, and the mobilization and fate of environmentally regulated metals, in both CO_2 storage complexes and overlying drinking water aquifers worldwide.

Keywords: Surat Basin, Evergreen Formation, seals, impure CO_2, CO_2 geological storage

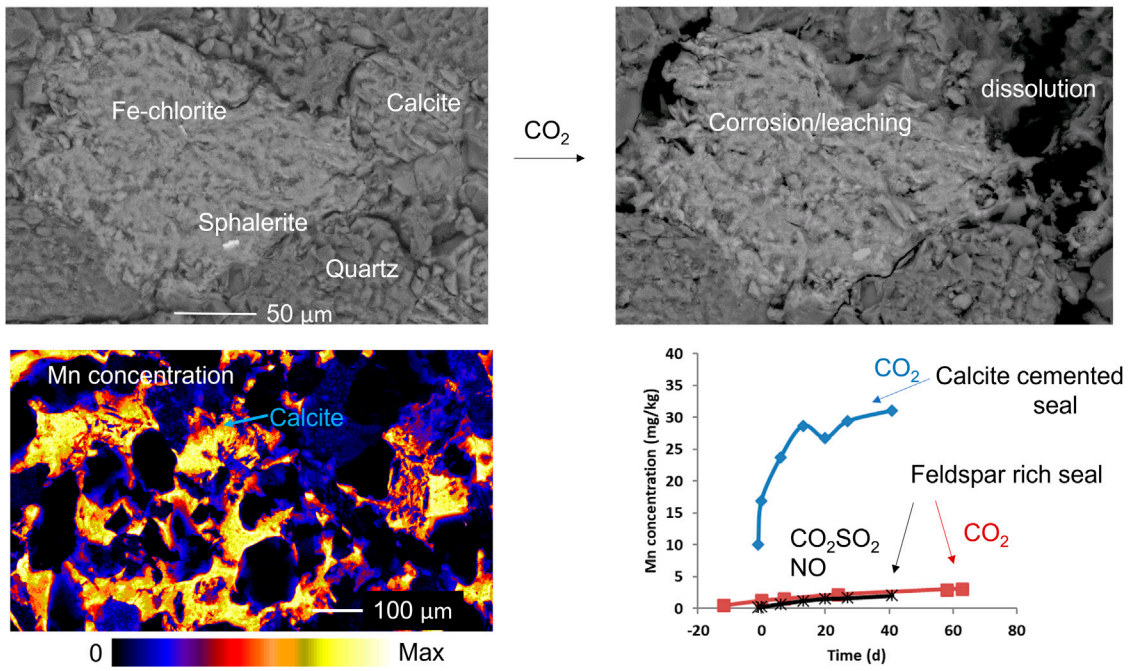

GRAPHICAL ABSTRACT |

INTRODUCTION

CO_2 geological storage has been identified as a vital part of the transition to lower greenhouse gas emissions. In a traditional sense, CO_2 geological storage involves injection of CO_2 into deep saline reservoirs or depleted oil and gas reservoirs overlain by a low permeability seal or caprock (Bachu et al., 1994; Alemu et al., 2011; Pearce and Dawson, 2018). CO_2-induced changes to reservoir water quality and rock properties are monitored in storage sites worldwide (Kharaka et al., 2006). Low-salinity, or drinking water, aquifers overlie the seals of several targeted or operational storage sites (Cahill et al., 2013; Humez et al., 2014; Cahill and Jakobsen, 2015). The potential impacts to these low-salinity aquifers, in the unlikely event of a CO_2 leakage, is one major risk factor often considered (Kharaka et al., 2006; Cheung et al., 2009; Kharaka et al., 2010; Kirsch et al., 2014; Kharaka et al., 2018). In some cases, the reservoir itself may be a low-salinity aquifer, in which case the potential short or long impacts around the storage site itself may be a concern (Hodgkinson and Grigorescu, 2012; Hayes et al., 2020). During geological storage, CO_2 will dissolve in formation water forming carbonic acid and causing acidification, the extent of which depends on the buffering capacity of the formation water and rock (Pearce et al., 2022c). This acidification may result in dissolution of rock-forming minerals and the release of metals from minerals or desorption of metals from mineral surfaces (Wunsch et al., 2013; Wunsch et al., 2014; Farquhar et al., 2015; Pearce et al., 2019b). Subsequent adsorption and precipitation processes can re-sequester metals so that there would only be a concern if the type and concentration of metals in formation water exceed regulations or guidelines and have the potential to cause lasting change or impact other users of the aquifer (Wigley et al., 2012; Pearce and Dawson, 2018; Pearce et al., 2018). CO_2 streams can be sourced from one or several industrial sources including coal combustion, natural gas processing, direct air capture, blue hydrogen production, and steel or cement production (Talman, 2015; Tsuji et al., 2021). These industrial CO_2 streams may contain impurities, such as ancillary gases including SOx, NOx, H_2S, O_2, or CH_4 (Porter et al., 2015; Harkin et al., 2017; Rütters et al., 2022). The trace metal mobilization response to impure CO_2 injection is even less well known than that from pure CO_2 injection (Pearce et al., 2015a; Marcon and Kaszuba, 2015; Pearce et al., 2019d). Real potential or perceived public concerns for the risk of CO_2 and brine or formation water leakage into low-salinity aquifers has led to recent interest in the potential impacts on water quality (Lawter et al., 2016; Kharaka et al., 2018; Pearce et al., 2019c). Recent work includes the study of natural sites of CO_2 accumulation and CO_2 or brine leakage up faults, fractures, or old wellbores (Viswanathan et al., 2012); field studies of deep or shallow CO_2 injection sites (Zheng et al., 2009; Yang et al., 2013); experimental studies of mineral reactions from drill core resulting in metal mobilization (Shao et al., 2014; Golding et al., 2019; Shao et al., 2020); and transport or geochemical modeling studies to predict if leakage could be expected and if metal mobilization would be of sufficient magnitude to cause a risk or if metals are re-sequestered by adsorption and re-precipitation of minerals (Carroll et al., 2014; Zheng et al., 2016; Pearce et al., 2021b).

Several studies have observed sandstone bleaching in the Carmel and Entrada caprocks by natural CO_2 and minor H_2S migration at Green River, Utah, near the Little Grand Wash Fault (Wigley et al., 2013; Kampman et al., 2016; Maskell et al., 2018). Dolomite, hematite, and K-feldspar dissolution was coupled to

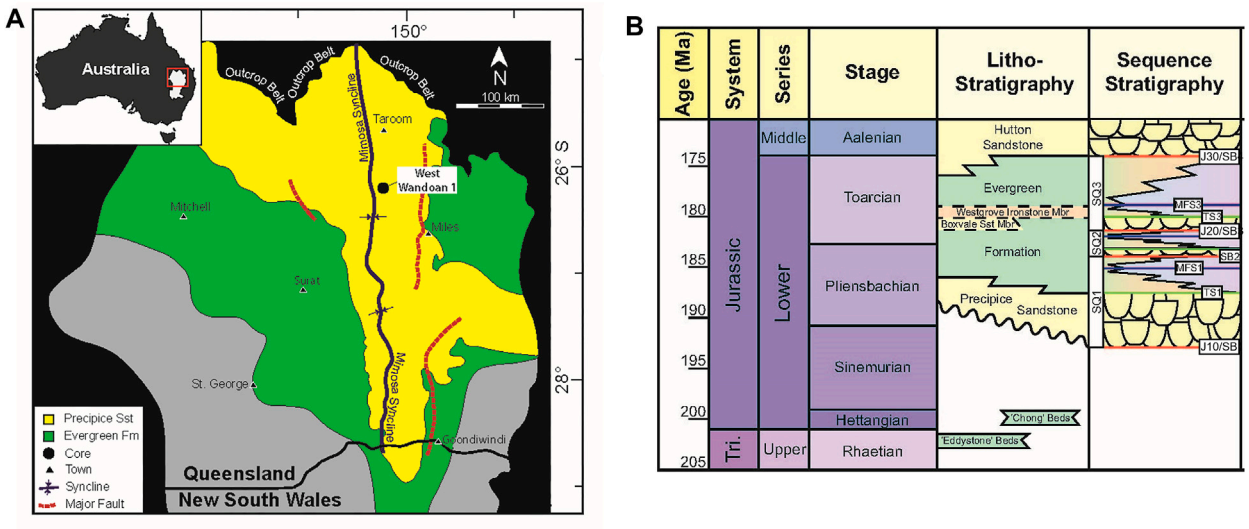

FIGURE 1 | (A) Map of the Surat Basin showing the West Wandoan 1 well. Note that the Evergreen Formation (green) extends over the Precipice Sandstone (yellow). **(B)** Litho- and sequence-stratigraphy of the Surat Basin where the Precipice Sandstone is the reservoir and the Evergreen Formation is the seal. The map and stratigraphy are modified after (La Croix et al., 2019a; La Croix et al., 2020b).

ankerite/Fe-dolomite, pyrite, hematite, chalcopyrite, and illite precipitation retarding CO_2 penetration. Several trace metals (including Fe, Cu, Ni, and Cr) were mobilized by dissolved CO_2 reaction; however, they were subsequently re-deposited in precipitates. The mobilization of Fe and Mn from calcite and iron oxyhydroxide was also reported in the saline Frio sandstone during a CO_2 field injection demonstration (Kharaka et al., 2006). However, the majority of experimental CO_2 reactions have reported major ion changes, but have not reported on minor and trace metals or regulated elements such as arsenic, and were generally only relevant to storage with pure CO_2. Experimental studies specifically looking at trace metal behavior have included reactions of limestone or dolomite with CO_2 (Wunsch et al., 2013; Wunsch et al., 2014). The main source of metals was determined to be from calcite dissolution, even though higher metal concentrations were locally present in pyrite or clay, with pyrite predicted to be an important source of metals at longer reaction time scales up to 30 years after carbonates reached saturation. CO_2-induced calcite dissolution and exchange reactions were also separately related to the mobilization of elements to solution from limestone core (Wang et al., 2016). One study performed drill core reactions with pure CO_2 in saline brines to monitor the metal release from a variety of reservoir and seal cores, including from sandstones, shales, carbonates, well cement, and basalt (Karamalidis et al., 2013). Reported increases in dissolved Fe and Mn concentrations from the carbonate cores occurred after CO_2 injection, Cr increased and subsequently decreased, and Pb generally increased but remained at low concentrations. The concentration of As, however, increased prior to CO_2 addition, indicating an additional desorption or ion exchange source (that can be an artifact of laboratory experiments). Separately, the Southwest Regional Carbon Sequestration Partnerships storage site seal, the Gothic Shale (consisting of clay, calcite, dolomite, quartz, and pyrite), and the carbonate reservoir minerals (dolomite, calcite, and minor pyrite) were reacted with CO_2 and brine in hydrothermal experiments to monitor metal release (Marcon and Kaszuba, 2015). The concentration of several metals including Fe, Ba, Pb, Co, Cu, Ni, Zn, and Cd increased initially on CO_2 reaction. Subsequently, the precipitation of pyrite, Co-sulfides, siderite, smectite, and oxide minerals decreased the dissolved concentrations of several metals including Pb, Cr, Co, and Zn. The shale caprock was found to be a source of metals but to also favorably provide secondary metal sinks. The above studies have focused on pure CO_2 injection under deep saline aquifer storage conditions; however, several low-salinity storage sites are currently being considered for geological storage. In addition if CO_2 were to leak to overlying freshwater or drinking water aquifers, water quality changes and metal mobilization could potentially occur (Choi, 2019). The ancillary gases in impure CO_2 streams can be a source for further acidification, oxidation, or changes in redox that may affect metal mobilization reactions. Therefore the study of metal mobilization in low-salinity aquifers, with pure or impure CO_2, is needed.

In the Surat Basin, Australia, a low-salinity reservoir, the Precipice Sandstone (**Figure 1**) has been investigated for a small-scale CO_2 injection demonstration in the northern region of the Glenhaven area. The West Wandoan 1 well was drilled for the feasibility study (**Figure 1**), where the CO_2 plume has been predicted to stay within the project boundary, which is a very small area of the overall tenement (tenement refers here to the licensed area of land) (Kirste et al., 2017; Golding et al., 2019; Kirste et al., 2019). The Evergreen Formation is the overlying seal

TABLE 1 | Summary of the samples and experiments. X = characterization was performed. Reacted samples include the reaction gas in the sample name as shown here.

Sample	1022.40 m	1043.70 m	1056.03 m
Type	Ironstone	Feldspar-rich Ss	Calcite cemented Ss
Total digestion	x	x	x
XFM	x	x	x
SEM	x	x	x
CO_2 reaction		1043.70 m CO_2	1056.03 m CO_2
CO_2SO_2NO reaction		1043.70 m CO_2SO_2NO	

complex consisting of a series of sandstones and low-permeability mudstone units of variable porosity, permeability, and mineralogy (Golab et al., 2015; Pearce et al., 2016; La Croix et al., 2019b). The Westgrove Ironstone Member is located within the Evergreen Formation (**Figure 1**), and is also considered a regional-scale seal (La Croix et al., 2019a; La Croix et al., 2020a; La Croix et al., 2020b; Pearce et al., 2021c). The Hutton Sandstone is the low-salinity aquifer overlying the Evergreen Formation, and in other areas of the Surat Basin, both the Hutton Sandstone and the Precipice Sandstone are sources of water for agriculture, mining, livestock, or town water bores (Suckow et al., 2018; Hayes et al., 2020). The native quality of the groundwater within these aquifers is very variable with location, being fresh to brackish near recharge in the northern part of the basin, but less well known in the deeper southern part of the Surat Basin, which is now being considered for large-scale CO_2 storage (Hodgkinson and Grigorescu, 2012; Feitz et al., 2014; Pearce et al., 2019a; Pearce et al., 2020; Pearce et al., 2022b). In addition, CO_2-enhanced oil recovery and storage is being considered in the Moonie Oil Field in the southern Surat Basin (Barakat et al., 2019; Pearce et al., 2021a). The initial source of local CO_2 is expected to be a coal-fired power plant, and after purification, the CO_2 stream is expected to contain low concentrations of ancillary gases including SO_2 and nitic oxide (NO) (and potentially O_2) which, when dissolved in formation water, can be more reactive to minerals than pure CO_2 owing to further acidification or changes in redox (Pearce et al., 2015b; Porter et al., 2015; Talman, 2015).

The potential for changes to aquifer water quality is a risk factor considered in environmental impact assessments of CO_2 storage sites. However, studies of CO_2-induced metal mobilization and fate in low-salinity storage complexes have generally been limited to shallow sites. Several field tests of very shallow CO_2 injection into alluvium at a depth of ~ 1.5–3 m, to understand potential CO_2 leakage at the Zert test site, reported increased dissolved concentrations of Ca, Mg, Fe, and Mn, with changes in pH, alkalinity, and electrical conductivity (EC) and small increases in trace metal concentrations including Pb and As (Kharaka et al., 2010; Kharaka et al., 2018). Experimental CO_2 reactions of the sediments attributed the dissolved metals to calcite, dolomite, and Mn-oxyhydroxide dissolution and to clay and oxide desorption or ion exchange processes (Kharaka et al., 2018). Studies of metal mobilization at low-salinity sites at typical storage depths of >800 m, however, are generally lacking.

This study has characterized the total and mineral-specific metal content of Evergreen Formation seal cores from a deep low-salinity injection target site in the Surat Basin. The geochemical response of the seal cores to experimental reaction with pure CO_2, and CO_2-containing SO_2 and NO, is assessed under CO_2 storage conditions. The mobilization of metals from the seals during the experimental reactions and the significance for CO_2 storage sites are discussed.

METHODS

Sixteen Evergreen Formation drill cores from the West Wandoan 1 well were powdered and subject to fusion and total acid digestion for major, minor, and trace element concentrations using previously reported methods (Golding et al., 2019). Inductively coupled plasma optical emission spectroscopy (ICP-OES) was used for major and minor elements, with inductively coupled plasma mass spectroscopy used (ICP-MS) for trace elements. Scanning electron microscopy with energy dispersive spectrometry (SEM-EDS) was performed in back scatter electron mode using a low-vacuum JEOL6460LA environmental SEM or a Hitachi TM3030 with a Bruker EDS. SEM-EDS was performed on both uncoated polished thin sections and on the core blocks, both pre- and post-reaction to directly observe any mineral alteration and corrosion. Images and elemental spectra of mineral surface spot analyses were obtained.

Three cores (ironstone 1022.40 m, feldspar-rich sandstone 1043.70 m, and calcite cemented sandstone 1056.03 m, **Table 1**) were prepared as thin sections on fused quartz slides for X-ray fluorescence microscopy (XFM) at the XFM beamline of the Australian synchrotron. Quartz slides were used since standard glass slides may contain a background of trace metals including As that can interfere with the analysis. A range of major, minor, and trace metals were detected at a spatial resolution of up to 2 μm, and at a dwell time of 10 msec/pixel including Fe, Ca, Mn, K, Ti, Ni, Cr, Pb, As, Sr, Zr, Zn, and Rb. Thin sections were attached using Mylar tape to a Perspex plate sample holder and mounted to the instrument translation stage. Scanning fluorescence microscopy was performed on the fly, using an X-ray beam (18.5 KeV) focused with Kirkpatrick–Baez mirrors to ~ 2 μm and using the Maia detector to produce fluorescence maps. Foil standards were run daily to calibrate elemental concentrations, with the instrument described in detail previously (Ryan et al., 2010; Paterson et al., 2011; Ryan et al., 2014). False color images of

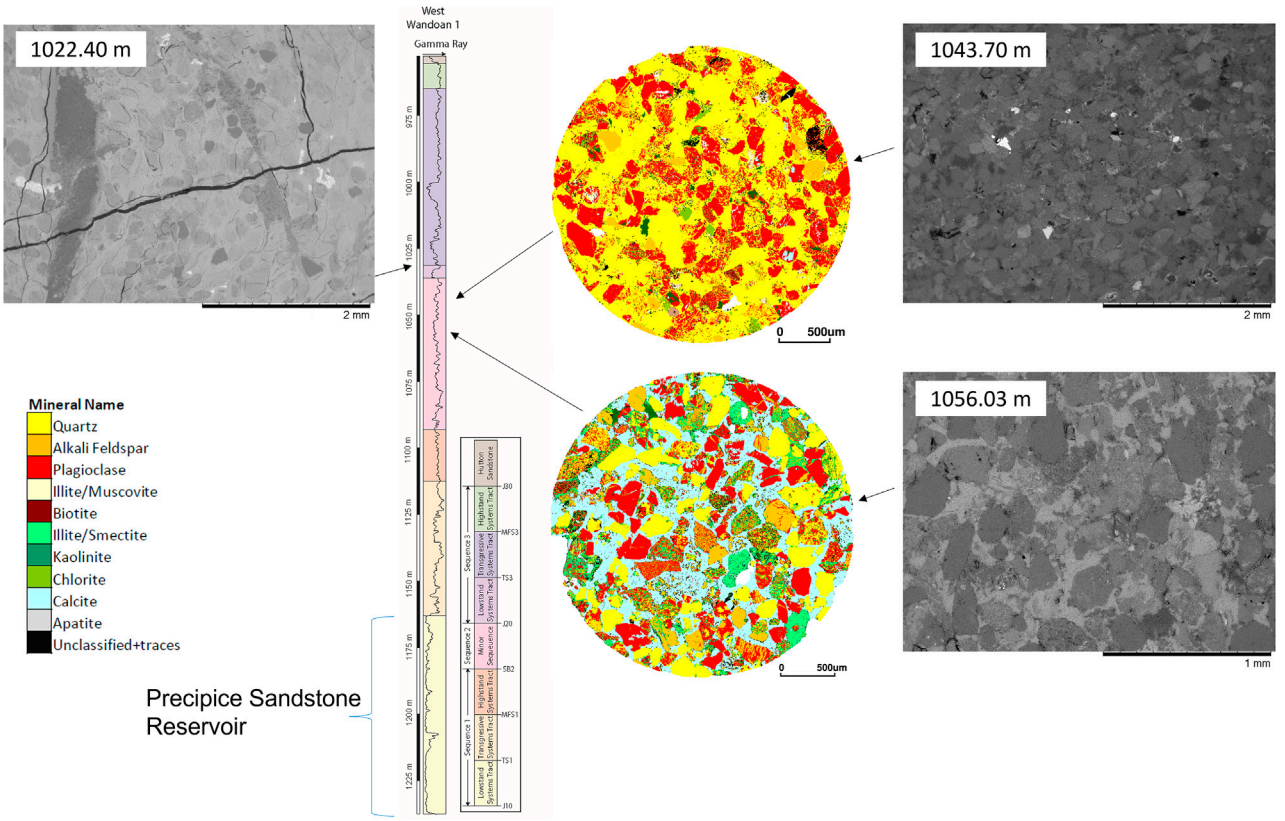

FIGURE 2 | SEM and QEMSCAN images of the Evergreen Formation samples with the QEMSCAN legend. The West Wandoan 1 well gamma ray log is shown for the Precipice Sandstone reservoir and overlying Evergreen Formation. Immediately overlying the Precipice Sandstone is a transition zone region, and above that are the seals of the Evergreen Formation. The sequence stratigraphy and nomenclature are based on the UQ-SDAAP modified from (La Croix et al., 2020b). See also the log given in the **Supplementary Material**.

concentration distributions and quantified concentrations over mineral areas were generated from the raw data using the software GeoPIXIE (CSIRO, 2011). Note that several light elements were not measured/imaged including Si, Al, Mg, and S. Subsequently, the same areas mapped were imaged by SEM-EDS to confirm the mineral phases hosting metals; this was especially important for clays and sulfides since Si, Al, and S were not imaged in XFM (Pearce et al., 2021a).

Batch experiments were performed using unstirred Parr® reactors with custom-built thermoplastic vessel liners, sample holders, and a dip tube assembly to avoid corrosion. The pressure and temperature of the vessels were monitored, with control and safety shutoff systems incorporated through a dedicated LabVIEW program. The vessels were maintained at 60 ± 1°C using heating jackets and thermostats, and the vessel pressure was monitored using pressure transducers. A fully contained pressurization system used a Teledyne ISCO syringe pump (500HP) to obtain a vessel pressure of 12 MPa to replicate *in situ* conditions in the Surat Basin.

In the experiments, either pure supercritical CO_2 or a CO_2SO_2NO gas mixture (**Table 1**) was used to replicate a possible post-combustion capture gas composition (Porter et al., 2015). Core 15-mm cubes and offcuts of either feldspar-rich sandstone (1043.70 m) or calcite cemented sandstone (1056.03 m) from the Evergreen Formation seals of the West Wandoan 1 well were used (**Table 1**). Rock core sub-sections were immersed in 100 ml of low-salinity water replicating a simplified expected composition of groundwater in the storage reservoir of the Glenhaven site where the West Wandoan 1 well is situated. The water consisted of 50 mg/kg NaCl and 148 mg/kg $NaHCO_3$ at an initial pH of 7.55. Reactor vessels were purged of residual air with a low-pressure N_2 flush. They were subsequently pressurized to 12.0 ± 0.5 MPa, initially with N_2 gas at a temperature of 60°C. A baseline water–rock reaction period with the inert N_2 gas was performed during which water samples were obtained to determine if any metals were released prior to CO_2 injection. The N_2 gas was subsequently replaced with either pure CO_2 gas or a gas mixture of 10 ppm SO_2 and 50 ppm NO in a balance of CO_2 using the syringe pump.

The solution pH of sampled water was measured immediately *ex situ* using a TPS WP81 meter and probes with an error of ±0.01 pH units, and conductivity was also measured. Water aliquots were diluted 20 times and acidified with pure HNO_3 for analysis. An ICP-OES (Perkin Elmer Optima 3300 DV) with an error of ~5% was used to measure major elemental concentrations of aqueous species. Trace element concentrations were measured by ICP-MS (Agilent 7900 ICP-MS with a collision cell) with errors of

TABLE 2 | Mineral content (%) of the Evergreen Formation samples from XRD and QEMSCAN, where "a" and "b" are two adjacent sub-sample areas. Micro CT and MICP porosity (%) is also shown where measured. XRD was performed on a powdered section of core as reported previously (Golding et al., 2019). QEMSCAN minerals and porosities were also reported previously (Pearce et al., 2019b).

	XRD	QEMSCAN a	QEMSCAN b	XRD	QEMSCAN a	QEMSCAN b	XRD
Depth (m)	1022.40	1043.70	1043.70	1043.70–1043.77	1056.10	1056.10	1056.03–1056.19
Quartz	3	57.6	61	42.3	21	25	27.3
K-feldspar		5.4	3.4	6.2	11.8	13	6.1
Plagioclase		26.6	22.3	22.3#	21.6	17.7	27.6#
Na-Ca plagioclase				18#			12.9#
Ca-Na plagioclase				12.3#			14.7#
Muscovite/illite	4.4	1.7	2.3	14.7	0.2	0.4	19.3
Biotite		1.4	1.2		0	0	
Illite-smectite		0	0		9.2	11.9	0.9
Kaolinite	8.2	0.9	2.8	2.9	0.6	0.9	2.1
Chlorite	4.6	3.1	3.8		0.8	0.9	
Calcite		0.3	0.5	0.7	30.1	25.2	16.3
Ankerite							0.5
Apatite	11	0.1					
Rutile		0.2					
Fe-hydroxide				2.9			
Siderite	63						
Unclassified	5.6*	2.7	2.2		4.7	4.9	
μCT % porosity		3.9	8.1		6.8	7.4	
MICP % porosity				5.5			8.2

*# Na-rich and Ca-rich plagioclase components from XRD. * Sulfide/pyrite cement. K-feldspar was identified as orthoclase in XRD.*

TABLE 3 | Rock total element digest data (mg/kg) for the three cores. Data for a wider range of Evergreen Formation samples from the West Wandoan 1 well core are in the **Supplementary Material**. Rock total trace element and rare earth element (REE) digest data (mg/kg) for the three West Wandoan 1 Evergreen Formation cores are also shown.

Depth (m)	1022.40 m	1043.70 m	1056.03 m	Depth (m)	1022.40 m	1043.70 m	1056.03 m
Li	32	26	20	Zr	83	119	119
Na	1521	20,155	13,231	Hf	1.9	2.9	3
K	1570	20,398	20,360	V	399	51	72
Rb	9.8	58	101	Nb	3.2	9.7	9.5
Cs	1	1.9	2.7	Ta	0.1	0.5	0.5
Be	3.2	0.9	1.5	Cr	26	25	24
Mg	1843	3,250	2,735	Mo	2.3	0.8	0.4
Ca	9,514	14,059	82,123	W	0.2	1	0.8
Sr	238	314	328	Mn	21,662	398	4,538
Ba	336	972	695	Fe	299,283	21,160	15,236
Sc	7.8	8.2	10	Co	156	9.6	12
Y	62	16	19	Ni	105	9.1	9.8
Th	3	10	6.9	Cu	20	19	8.5
U	2.2	1.6	1.5	Al	33,029	64,846	59,634
Ti	1530	7,439	3,276	Si	51,195	341,929	264,843
Ag	<DL	0.02	0.02	La	56	28	29
Zn	105	70	67	Ce	136	61	63
Cd	0.4	0.09	0.1	Pr	14	6.8	6.6
Tl	2.7	0.5	0.7	Nd	60	28	26
Ga	12	16	18	Sm	13	5.3	4.9
Ge	3.7	1.5	1	Eu	3.1	1.3	1.6
Sn	0.9	1.6	1.5	Gd	13	5	5
Pb	34	12	16	Tb	2	0.6	0.6
Bi	0.2	0.06	0.08	Dy	12	3.2	3.5
As	62	8.6	6.2	Ho	2.6	0.6	0.7
Sb	1.3	0.3	0.4	Er	8.3	1.7	1.9
P	1856	925	655	Tm	1.4	0.2	0.3
S	4,762	257	427	Yb	10	1.6	1.8
Se	1.1	0.08	0.1	Lu	1.5	0.3	0.3
				Total REE	333	143	145

TABLE 4 | Summary of XFM observations of the main mineral hosts of selected metals in three cores. Elements in brackets; for example, (Cr) indicates that Cr was present in some garnet grains. Major element associations and further data are given in the **Supplementary Material**.

	1022.40 m	1043.70 m	1056.03 m
Mineral host	Ironstone	Feldspar rich Ss	Calcite cemented Ss
Siderite	Mn, Pb, Sr (Cr)		
Calcite	Mn, Sr	Mn, (As), (Sr)	Mn, Sr
Chlorite	Mn, Cr, Rb, Sr	Mn, Rb, Sr, Zn (Cr)	
NaCa-plagioclase	Sr		
Ca-plagioclase		Sr	
K-feldspar	Sr	Rb, Sr, Pb	Rb, Pb
Illite/muscovite/biotite	Rb	Rb, Sr, Zn, Mn	
Garnet	Mn, Zn, (Cr)		
Pyrite cement	As, Pb, Cr		As, Zn, Pb
Sphalerite/ZnFe sulfide		Cu, Zn, Ni	
Apatite cement	Sr, (As)		
Vein mixed sulfide cements	Sr, Ni, Cu, As, Pb		

less than 10%. Further details of the experiment set up have been published previously (Pearce et al., 2015a; Turner et al., 2016; Pearce et al., 2019b).

RESULTS

The three core samples are from the West Wandoan 1 well, from the Evergreen Formation seals. An ironstone, from 1022.40 m, part of the Westgrove Ironstone Member regional seal (**Figures 1**, **2**; **Table 2**), contained abundant siderite cement, with a silica- and calcite-cemented natural fracture and with accessory pyrite and apatite cements. The feldspar-rich sandstone, 1043.70 m, was a feldspar- and clay-rich sandstone, with localized small veins containing mixed rutile and sulfide cements. The sample from 1056.03 m was a calcite cemented sandstone that also contained a high proportion of plagioclase feldspar, K-feldspar, and clays including illite and Fe-rich chlorite (**Figure 2**; **Table 2**). QEMSCAN images of the 1043.70-m and 1056.03-m samples are shown in **Figure 2**. Mineral compositions reported from QEMSCAN analysis and X-ray diffraction (XRD) are given in **Table 2**, with the porosities from mercury injection capillary porosimetry (MICP) and micro-computed tomography (μ-CT) (Pearce et al., 2019b).

Total concentrations of elements in the three samples from whole rock acid digestion are given in **Table 3**. Total element data for a wider range of sixteen core samples from the Evergreen Formation are also given in the supplementary material with the core description (**Supplementary Tables S1, S2**). In the three main samples discussed here, total core Mn content from the acid digestion was highest in the two carbonate cemented rocks, the siderite cemented ironstone from 1022.40 m, and the calcite cemented sandstone from 1056.03 m. Total concentrations of Co, Ni, and Cu were higher in the ironstone (1022.40 m) that contained pyrite cements (**Table 3**). U was generally <2.2 mg/kg in the three samples. Cr was comparable in the three cores at 24–26 mg/kg. Total Zn was 105, 70, and 67 mg/kg at 1022.40, 1043.70, and 1056.03 m, respectively. Total Pb was 34, 12, and 16 mg/kg, respectively, and As was 62, 8.6, and 6.2 mg/kg (**Table 3**). Rb was 9.8, 58, and 101 mg/kg at 1022.40, 1043.70, and 1056.03 m, respectively. Total Sr content at 1022.40, 1043.70, and 1056.03 m was 238, 314, and 328 mg/kg, respectively.

XFM Characterization

XFM observations are summarized in **Table 4**, with the concentrations given in **Supplementary Table S3**. Additional images are in the **Supplementary Material**. In the XFM-scanned thin section of feldspar-rich 1043.70 m, metals such as Pb, As, Ti, and Ni were concentrated in veined regions (**Figure 3**). Vein-hosted Ti-oxide cements and sulfide cements were associated in similar regions but spatially separate (**Supplementary Material**). Apatite cements were additionally mixed with the sulfide cement. Metals such as Mn were hosted in traces of calcite cement and chlorite throughout 1043.70 m. In addition, rare garnet grains and mixed composition cements contained Mn. Rb was associated with K-feldspars and also with illite and the occasional mica. Sr was present in vein cements, in NaCa-plagioclase feldspars, and in calcite. Rare barite cements were also present. Cr was present in some garnet grains.

The ironstone, 1022.40 m, contained the highest concentrations of As in pyrite cements (**Figure 3**; **Table 4**, and **Supplementary Material**). Both calcite and siderite cements contained Mn, which was more concentrated in siderite. Siderite additionally hosted Pb. Sr was in apatite cement, K-feldspar, and siderite in decreasing amounts (**Table 4**, **Supplementary Table S3**).

The calcite cemented sandstone from 1056.03 m hosted Mn mainly in calcite and, additionally, in chlorite (**Supplementary Material**). Rb was hosted in K-feldspar and chlorite. Cu, Zn, Pb, and Ni were concentrated in pyrite- or sphalerite-mixed sulfide cements (**Figure 4**). Sr was concentrated in plagioclase but also present in calcite cement.

Gas–Water–Rock Reactions

Rock Surface Alteration

SEM images of the 1043.70-m core block surfaces before and after reaction with CO_2 and formation water are shown in **Figure 5** and **Supplementary Material** (**Supplementary Figures S9–S11**). After reaction, calcite cements had dissolved (**Figure 5D**), and Ca-Na-plagioclase and chlorite were corroded or altered (**Figures**

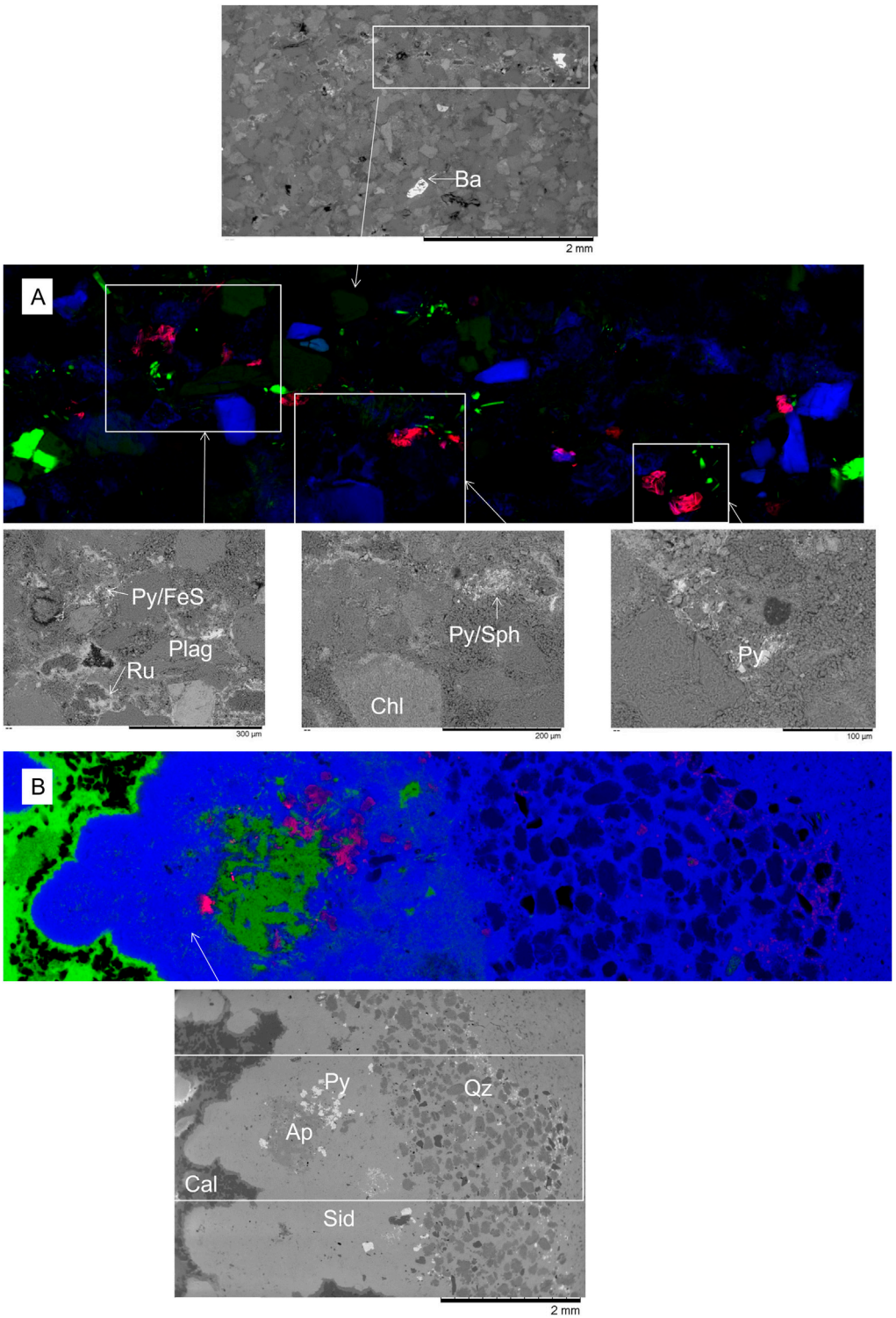

FIGURE 3 | (A) XFM image of feldspar-rich sandstone from 1043.70 m where red = As, green = Ca, and blue = Fe. Maximum concentration shown of As = 0.97%, Ca = 30.4%, and Fe = 33.8% in the image. **(B)** XFM image of ironstone from 1022.40 m where As = 0.96%, Ca = 94.4%, and Fe = 75.1% in the image. Associated SEM images of areas are shown of the white boxed areas, with Ba, barite cement; Py, pyrite cement; Sph, sphalerite cement; Ru, rutile cement; Chl, chlorite; Pla, plagioclase; Cal, calcite; Sid, siderite; Ap, apatite cement; Qz, quartz grains.

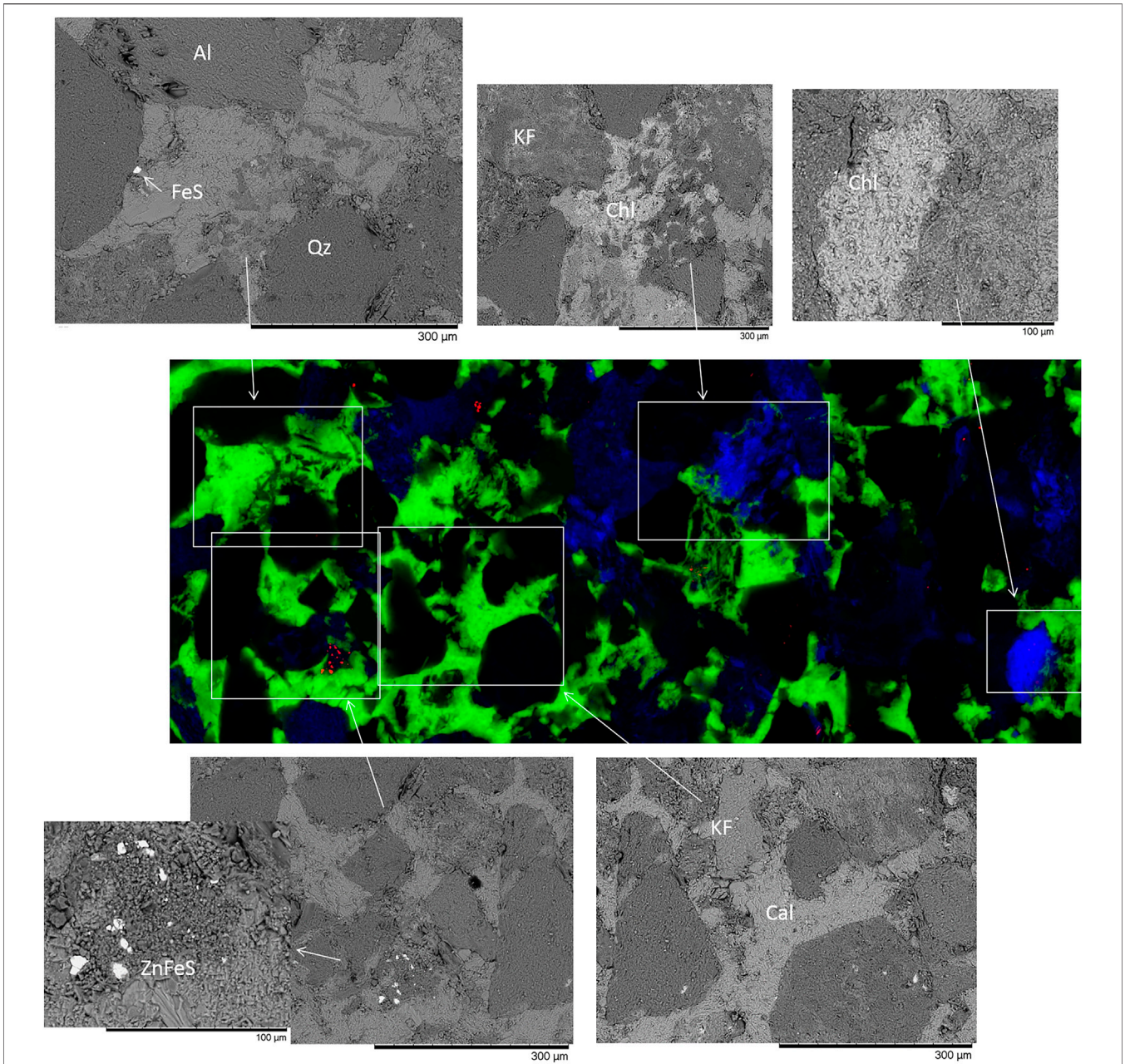

FIGURE 4 | XFM image of calcite cemented from 1056.03 m where red = Zn, green = Ca, and blue = Fe. The maximum concentrations shown are Zn = 6.54%, Ca = 91.8%, and Fe = 36.8%. Associated SEM images of mineral areas in white boxes are also shown. FeS, FeSx/pyrite cement + Cu. Qz, quartz; KF, K-feldspar; Chl, chlorite; Cal, calcite. ZnFeS, mixed sphalerite or ZnFe-sulfide that also contained Ni.

5D,F). In addition, muscovite was slightly corroded or delaminated, and illite and kaolinite were locally corroded or altered (**Supplementary Material**). Some fine-grained sulfides appeared to have corroded or migrated from surfaces as fine particles.

After the reaction of feldspar-rich sandstone, 1043.70 m, with CO_2SO_2NO and formation water, calcite cements had dissolved, and chlorite had corroded or altered (**Supplementary Figures S12–S14**). Apatite and pyrite cements, however, were additionally corroded (**Figures 6A–D**), along with some mixed sulfide cements associated with veins.

The calcite cemented core from 1056.03 m was also reacted with CO_2 and formation water (**Figures 6E–H**). The most obvious change was the dissolution of calcite cement revealing grain boundaries and pore-filling clays (**Figures 6E,F**, and **Supplementary Material**). In addition, Fe-rich chlorite was somewhat corroded and the occasional fine-grained Zn- or Cu-sulfides were altered or corroded (**Supplementary**

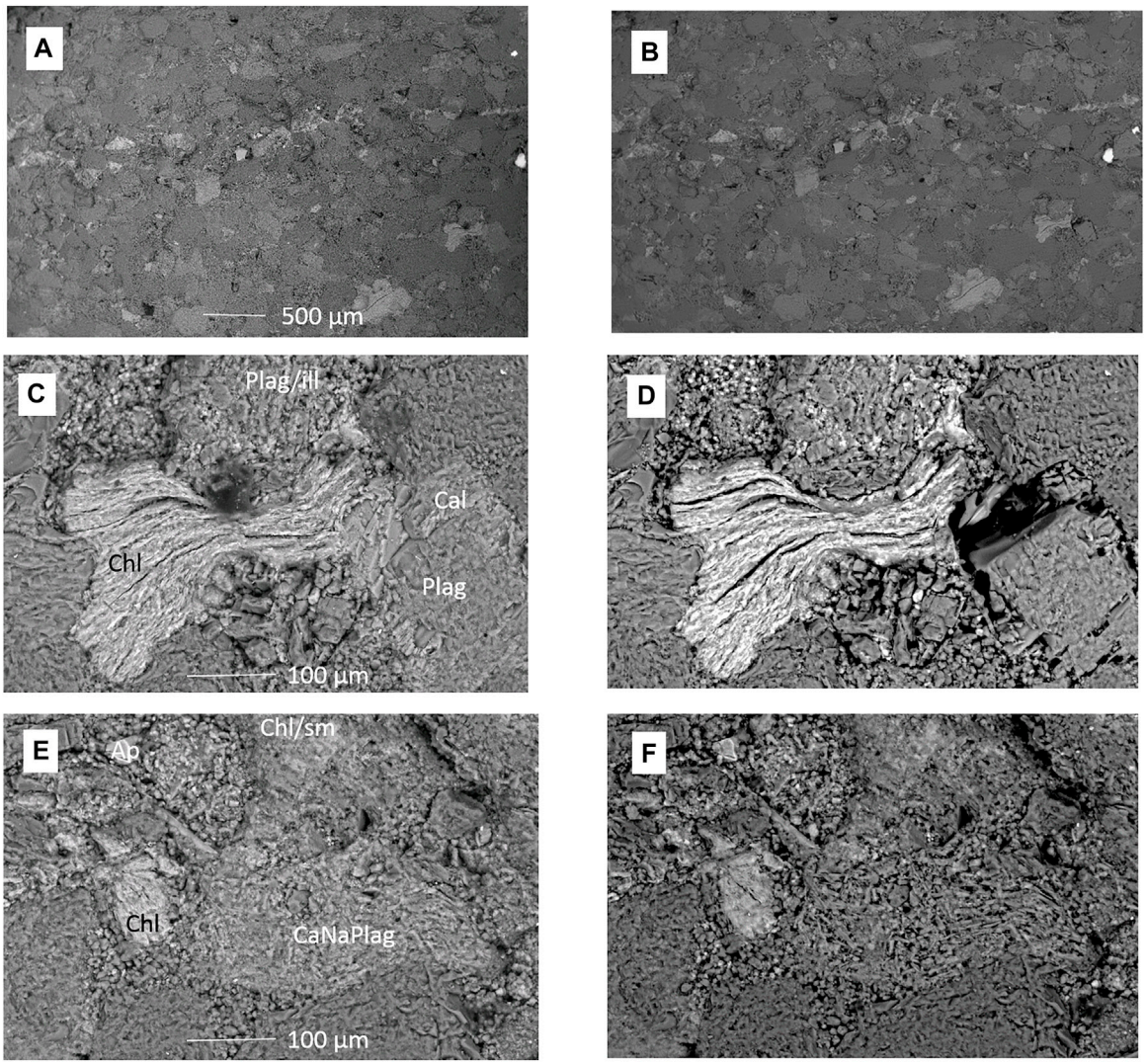

FIGURE 5 | SEM images of the feldspar-rich sandstone 1043.70 m core block surface before and after CO_2-formation water reaction. **(A)** Area showing a vein before reaction and **(B)** after reaction. **(C)** Chlorite, plagioclase, and calcite cement before reaction and **(D)** after reaction with calcite dissolved and chlorite altered. **(E)** Framework grains and clays before reaction and **(F)** after reaction with the Ca-Na-plagioclase (CaNaPlag) corroded. Plag, plagioclase; Cal, calcite; Chl, chlorite; Plag/ill, plagioclase and illite mix; Ap, apatite; Chl/sm, chlorite and smectite mixture.

Material). Rare FeMg-garnets and FeMgCr/Mn-garnets were present; however, they did not appear significantly corroded after reaction (**Supplementary Material**). Mixed Na-Ca-plagioclase also showed only minimal corrosion features (**Supplementary Material**). Zircon, rutile, and Fe-silicate cements appeared unaltered.

Dissolved Elements During Reactions

The dissolved element trends during the reactions are summarized in **Table 5**. The concentrations of several elements, including As and Cd, increased during the water–rock soak period, prior to the addition of CO_2. This represents ion exchange owing to dis-equilibrium and the difference between the native formation water and synthetic formation water, and it is an artifact of laboratory experiments.

On addition of pure CO_2 in the reaction of feldspar-rich sandstone from 1043.70 m, the pH decreased to 5.64 (**Figure 7**) and then varied slightly to 5.69 at the end of the experiment. The concentration of dissolved ions including Ca, Mn, Ba, Co, Si, Rb, and S increased and subsequently continued to increase or plateau (**Figure 7**, **Figure 8**; **Table 5**). Dissolved Fe, Cr, Ni, U, Pb, and Zn initially increased and subsequently decreased in concentration or, in the case of Zn, varied during reaction. The concentration of Cd generally increased prior to CO_2 addition from ion exchange and subsequently decreased over time (**Supplementary Material**). Prior to CO_2 addition, As concentration also increased and then continued to increase gradually, subsequently decreasing after 60 days. Dissolved Ca was correlated with both Mn and Mg, suggesting a similar source mineral, such as calcite (**Supplementary Material**). Ca was also

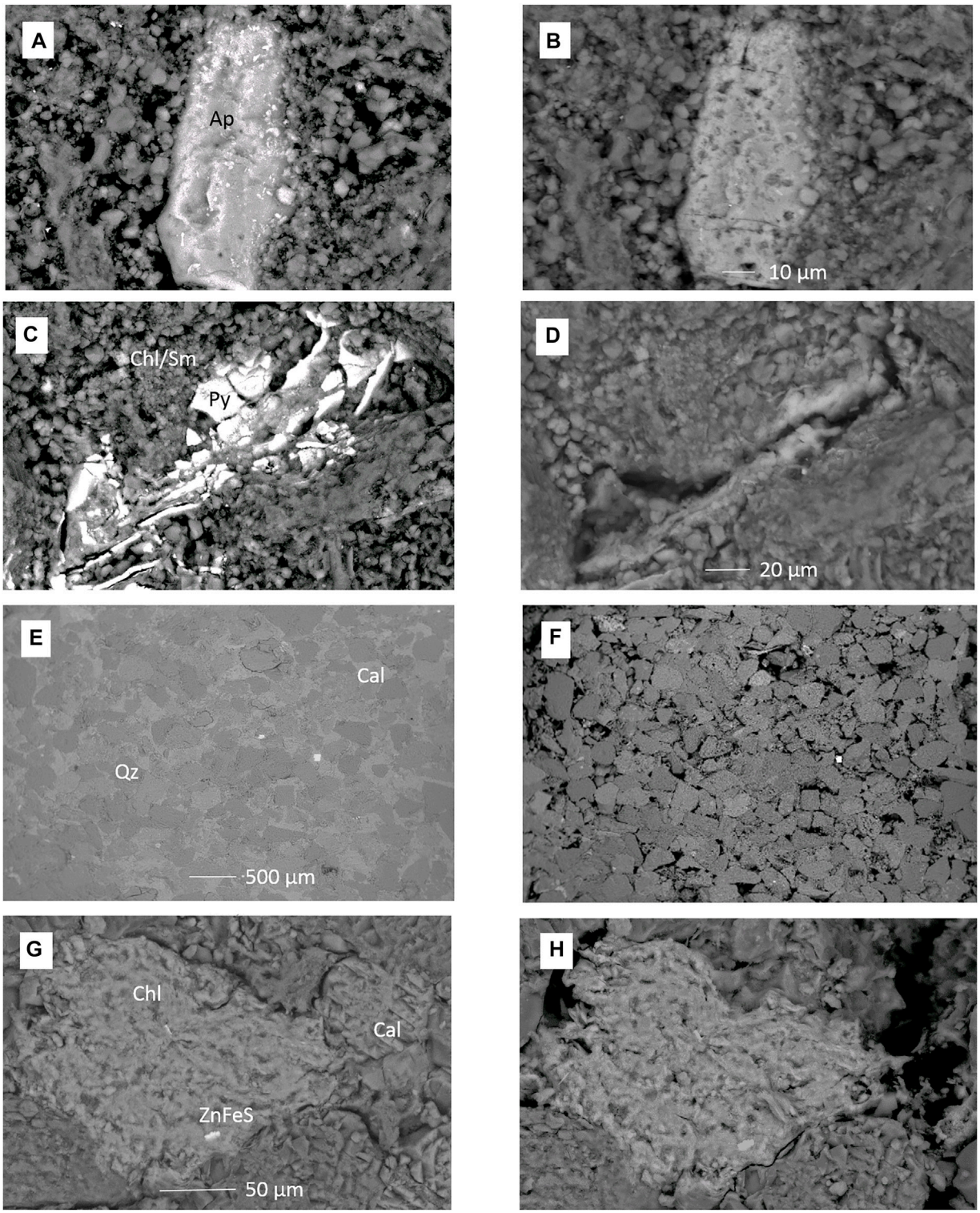

FIGURE 6 | SEM images of **(A–D)** feldspar-rich sandstone 1043.70 m before and after reaction with CO_2SO_2NO and formation water. **(A)** Apatite before reaction and **(B)** apatite corroded after reaction. **(C)** Pyrite cement in clay matrix before reaction and **(D)** pyrite dissolved or dislodged with clay fines from the surface after reaction. **(E–H)** Calcite cemented sandstone 1056.03 m before and after reaction with pure CO_2 and formation water. **(E)** Calcite cemented framework grains and **(F)** after reaction with calcite cements dissolved. **(G)** Chlorite, calcite cements, and ZnFeS cement. **(H)** After reaction with calcite dissolved, chlorite slightly corroded and ZnFeS corroded. Ap, apatite; Chl/Sm, mixed chlorite and smectite; Py, pyrite cement; Qz, quartz; Cal = calcite cement.

TABLE 5 | Summary of batch experiment trends of dissolved ions after CO_2 addition (unless otherwise specified). I = increase in concentration after CO_2 addition. I, S = increase and stabilization; D = decrease; I, D = increase and then decrease; V = varying; E = increase before CO_2 addition.

	1043.70 m CO_2	1043.70 m CO_2SO_2NO	1056.03 m CO_2
Dissolved element	Feldspar-rich Ss	Feldspar-rich Ss	Calcite cemented Ss
Ca	I, S	I, S	I
Mn	I, S	I, S	I
Mg	I, S	I, S	I
Fe	I, D	I, D	I, D
Ba	I, S	I, S	I
Co	I	I	I, S
Si	I	E, I	I
Rb	E, I	E, I, D	E, I, S
As	E, I, D	E, I, D	I, D
Pb	I, D	I, D	I, D
Zn	I, V	I, V	I, V
S	I, D	I, D	I, D
U	E, I, S	E, I, D	E, I, S
Cd	E, D	E, D	E, D
Al	I, D	E, I, D	I, D
Cs	I	I	E, I

correlated with Sr, Rb, Tl, Si, and Cs (**Supplementary Material**). Dissolved Pb was correlated with both U and S (**Supplementary Material**).

On reaction of feldspar-rich sandstone, 1043.70 m, with CO_2SO_2NO, the pH decreased to 5.75 and continued to decrease to 5.46 after 20 days, before increasing slightly to 6.01. Several dissolved elements had similar trends to the pure CO_2 reaction of the same sample. The dissolved concentrations of U, Pb, As, Cd, Ni, and S, however, generally had greater increases in concentrations initially, followed by generally decreasing trends (**Figure 8**, **Figure 9**, and **Supplementary Material**). Dissolved Ca concentration was correlated with Mn, Ba, Sr, Co, Rb, and Tl (**Supplementary Material**). Si and Co were correlated with each other; Ni and Cr were also correlated, as were Sr with Ba, and Pb with U (**Supplementary Material**).

On pure CO_2 reaction with the calcite cemented sandstone, 1056.03 m, the pH decreased to 6.35 and then to 6.18 after 20 days and subsequently increased to 7 (**Figure 7**). Increasing concentrations of dissolved elements including Ca, Mn, Sr, Ba, Rb, and Co were released (**Figure 7**, **Figure 8**, **Table 5**) and were at higher concentrations compared to the reactions of feldspar-rich sandstone at the Evergreen Formation from 1043.70 m. Generally, a lower concentration of As was released from calcite cemented sample, 1056.03 m, compared to the reactions of feldspar-rich 1043.70 m. Dissolved Pb, Cd, Cr, Ni, and Fe from 1056.03 m had variable but generally decreasing concentrations over time. Dissolved Ca was correlated with Mn, Sr, Mg, Rb, and U (**Supplementary Material**).

DISCUSSION

The caprock cores contained variable concentrations of total whole rock metals (**Table 3**, and **Supplementary Material**). The presence of a high total concentration of an element in the core, however, does not indicate that it will be mobilized on CO_2 reaction. For example, the Ba content was high in all rocks (**Table 3**); however, <2 and <6% were released in the reactions (**Table 5**), likely owing to the majority of Ba hosted in insoluble barite. In the three cores characterised by synchrotron XFM, several metals, such as Mn, were hosted in multiple mineral types including calcite, siderite, and chlorite. Pb was hosted in sulfides and siderite, As was hosted in sulfides and locally in apatite cements. Rb was in K-feldspar, plagioclase, and clays. Sr was hosted in carbonates, Ca-plagioclase, and apatite vein cements.

The water chemistry during the reaction of the calcite cemented sandstone, 1056.03 m, with CO_2 reaction was dominated by calcite cement dissolution with a continued increase in dissolved Ca, Mg, Mn, Co, and Sr concentrations from calcite. Since the pH was buffered by calcite dissolution, less reaction of silicate minerals occurred than during the reaction of calcite-poor, feldspar-rich sandstone from 1043.70 m. Chlorite, however, did show reaction features in SEM and likely contributed to increasing Fe, Mg, Co, Rb, and Mn concentrations (Armitage et al., 2013). Subsequent decreases in Fe over time indicate the precipitation of Fe-(hydr) oxide (or siderite). Precipitates were, however, observed as brown coatings on the rock samples and were not in high enough abundance for direct observation and identification or characterization through SEM in these experiments. We have previously observed precipitated fine-grained Fe-oxides in similar experiments with reservoir sandstones where NO or traces of air may act as an oxidation source (Turner et al., 2016). Fe-oxide precipitation was also reported in caprock reactions with CO_2 and O_2 (Shao et al., 2014) and with CO_2, SO_2, and O_2 (Pearce et al., 2016; Pearce et al., 2019d). The dissolved concentration of Zn increased from the observed reaction of ZnFe-sulfide cements in the current experiments. Dissolved concentrations of As and Pb generally remained relatively low during reaction of 1056.03 m, likely *via* being re-sequestered or adsorbed on calcite surfaces and in precipitating minerals such as Fe-hydroxides or siderite coatings (Román-Ross et al., 2006).

A lower solution pH was generated during the pure CO_2 reaction of feldspar-rich from 1043.70 m that contained a smaller

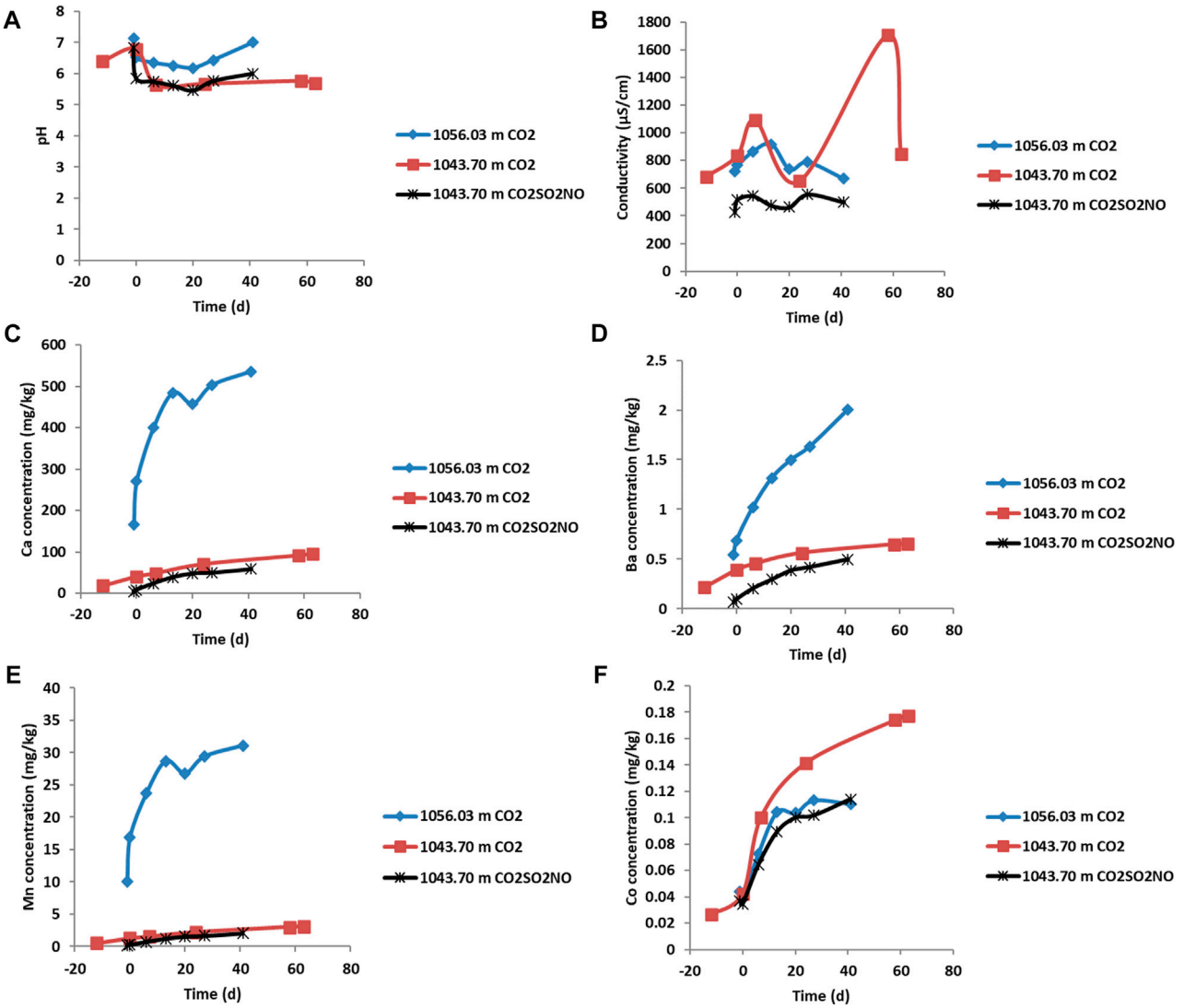

FIGURE 7 | Water quality parameters and dissolved element concentrations (mg/kg) during the reactions of Evergreen Formation core with CO_2 or CO_2SO_2NO. The negative time points represent the water composition and water rock interaction, and the CO_2 gas was introduced at time zero. **(A)** Solution pH, **(B)** electrical conductivity, **(C)** concentration of Ca, **(D)** Ba, **(E)** Mn, **(F)** Co. The concentrations have an error of 5% within the size of the symbols.

quantity of calcite cement than in the reaction of calcite cemented 1056.03 m. This resulted in less pH buffering for 1043.70 m than during the reaction of calcite cemented 1056.03 m. Therefore, for 1043.70 m, in addition to calcite dissolution, chlorite and Ca-Na-plagioclase also reacted, contributing to increasing dissolved concentrations of Ca, Mn, Sr, Mg, and Rb. On impure CO_2SO_2NO reaction of 1043.70 m, a lower pH was generated from the formation of stronger acids *via* dissolution of the impurity gases (**Eq. 1**). Calcite, chlorite, and Ca-Na-plagioclase reacted in addition to pyrite and apatite in the CO_2SO_2NO reaction of 1043.70 m. The lower pH and oxidative dissolution of pyrite by NO (or trace air) likely occurred in the presence of the impurity gases (Equ 2) (Shao et al., 2014). The concentrations of Pb, S, Cd, Ni, and U were initially higher in the CO_2SO_2NO experiment relative to the pure CO_2 reactions, and these elements were likely at least partially sourced from the observed additional reaction of sulfides and apatite. The concentration of Pb and U subsequently decreased during the CO_2SO_2NO reaction and stabilized during the pure CO_2 reaction, through incorporation in or adsorption on Fe-oxides (**Eq. 2**).

$$SO_2 + H_2O + \tfrac{1}{2}O_2 \rightarrow H_2SO_4 \quad (1)$$

$$FeS_2 15/4O_2 + 7/2H_2O \rightarrow Fe(OH)_3 + 2H_2SO_4 \quad (2)$$

Relatively few other studies have been performed on metal release with CO_2 reaction; however, they did also show that metals can subsequently be removed from solution during precipitation and adsorption, in agreement with the current study. Kampman measured metals from hematite dissolution and re-precipitation in a site of natural CO_2 and H_2S leakage at the

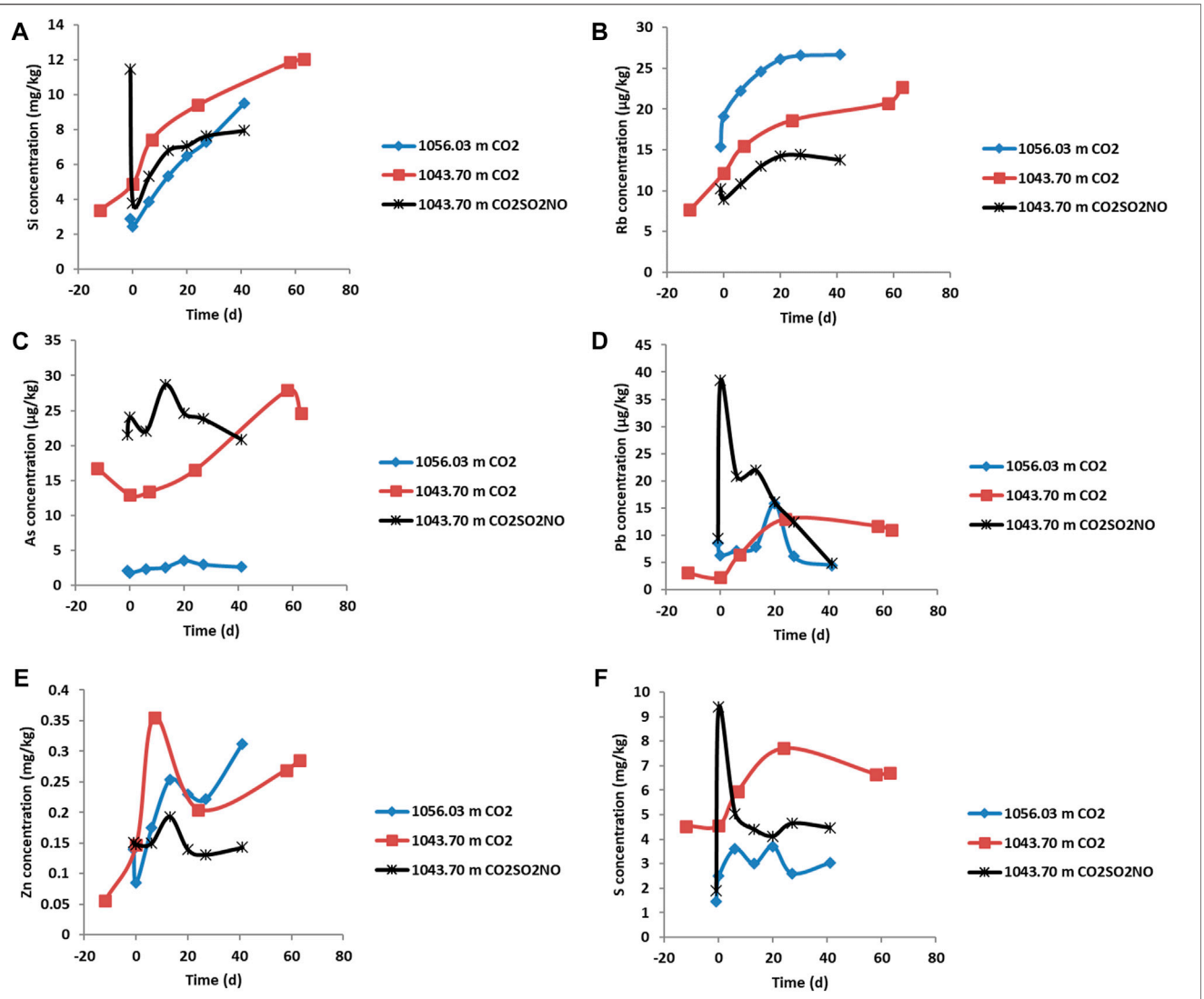

FIGURE 8 | Dissolved element concentrations during the reactions of Evergreen Formation core with CO_2 or CO_2SO_2NO. The negative time points represent the water composition and water rock interaction, and the CO_2 gas was introduced at time zero. **(A)** Concentration of Si (mg/kg), **(B)** Rb (µg/kg), **(C)** As (µg/kg), **(D)** Pb (µg/kg), **(E)** Zn (mg/kg), and **(F)** S (mg/kg).

Green River site, United States (Kampman et al., 2017). They observed that hematite was dissolved from bleached sandstone, with bands of re-precipitated Co, Cu, Zn, Pb, and Ni in carbonates and oxide minerals. Marcon and Kaszuba observed increases and subsequent decreases in dissolved Pb, Cr, Co, and Zn in CO_2 experiments reacting Gothic shale (Marcon and Kaszuba, 2015). Sulfides, siderite, smectite, and oxide minerals were precipitated. Separately, Eau Clair Formation siltstone caprocks were reacted with CO_2 and brine, and the release of Pb, As, Cd, Cu, etc. to the solution was also observed (Shao et al., 2014). Experiments with 5% O_2 in the CO_2 stream showed that sulfides were oxidized, resulting in a lowered pH, and Pb, Cd, and Cu increased. However, the precipitation of Fe-oxides resulted in lower concentrations of released As. Divalent cations such as Mn and Sr can be incorporated into carbonate minerals by substitution (Pingitore Jr et al., 1992; Wunsch et al., 2013; Wunsch et al., 2014). Incorporation of metals by precipitation or adsorption has also been documented for some non-CO_2 studies. Pb co-precipitation was measured, for example, in siderite (Erdem and Özverdi, 2005). Removal of As (III) from drinking water by natural siderite and hematite in batch and column experiments was also reported, where X-ray fluorescence showed As in Fe-oxide coatings on siderite (Guo et al., 2007). Synthetic siderite was also reported to sequester As, through the formation of Fe hydroxides under oxic conditions (Guo et al., 2011). An increase in As adsorption from 25 to 55°C was observed, where sulphate, nitrate, phosphate, or silica anions at concentrations less than 20 mg/kg were not competing for adsorption. As (III) has additionally been shown to adsorb on calcite surfaces and co-precipitate through sorption experiments and modeling at 20°C (Román-Ross et al., 2006). Roman-Ross found that As incorporation through co-precipitation was likely

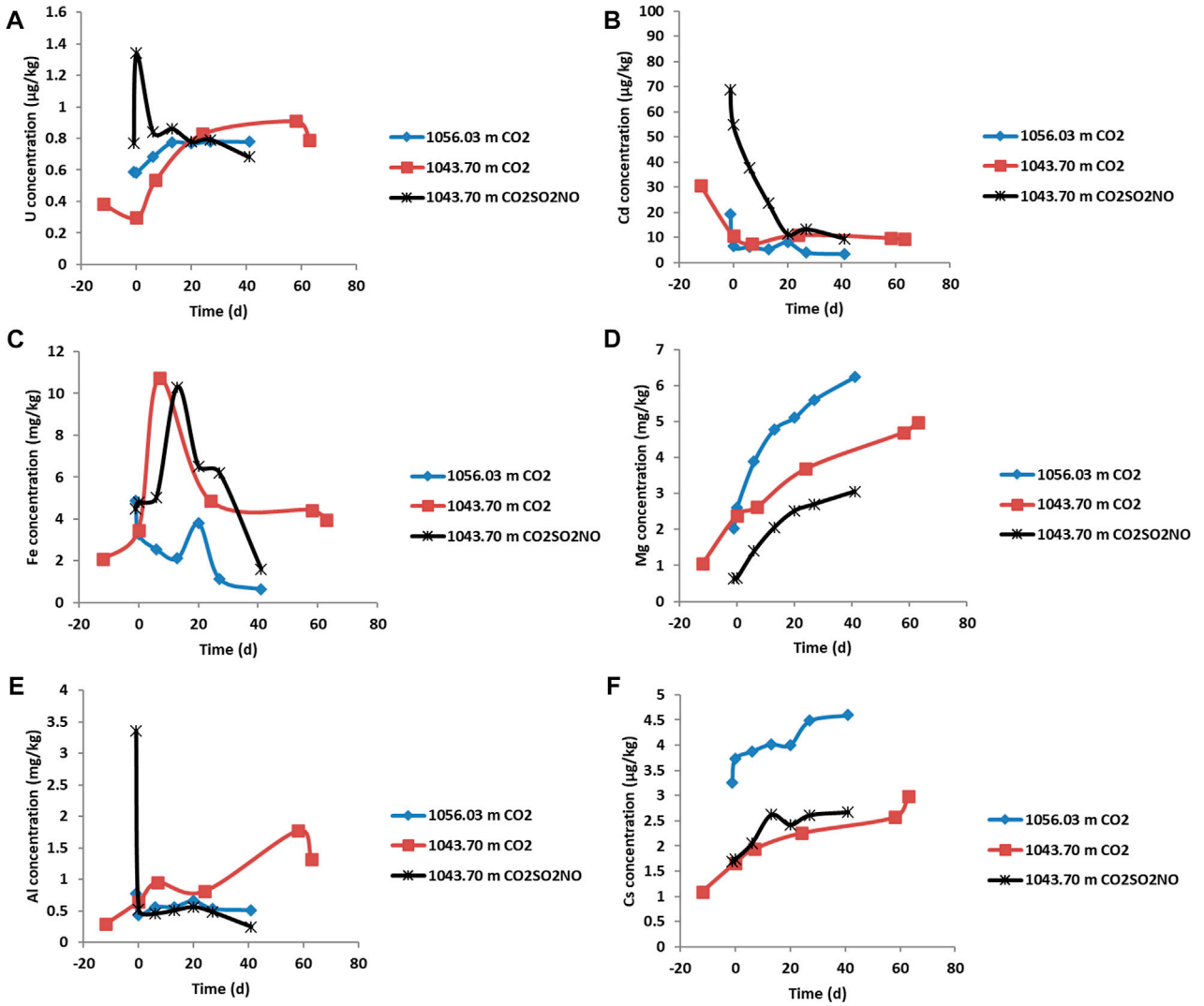

FIGURE 9 | Dissolved element concentrations during the reactions of Evergreen Formation core. The negative time points represent the water composition and water rock interaction, and the CO_2 gas was introduced at time zero. **(A)** Concentration of U (µg/kg), **(B)** Cd (µg/kg), **(C)** Fe (mg/kg), **(D)** Mg (mg/kg), **(E)** Al (mg/kg), and **(F)** Cs (µg/kg).

only limited by the As concentration available and that 30 mM/kg As could be incorporated. As, Cd, and Co were also reported to be adsorbed and co-precipitated in goethite precipitated at 25°C (Jiang et al., 2013).

The core samples may give insights into the expected longer-term reactions. The ironstone from 1022.40 m contained a natural fracture sealed with precipitated sulfide, apatite, silica, and reworked carbonate cements. It has been shown separately that the Mn-calcite in calcite cemented Evergreen Formation drill core from ~1056 m is also associated with fracture filling from past hydrothermal fluid near fault zones in the Surat Basin, and was most likely precipitated at 80–120°C (Golding et al., 2016). In addition, feldspar-rich sandstone from 1043.70 m had localized veins filled with mixed sulfide, rutile, apatite, and calcite cements. In these altered rocks, As has been sequestered in pyrite, Pb in siderite and sulfides, and Mn and Sr in calcite and siderite cements.

During the experimental reactions reported here, the amount of an element released as a percentage of the total concentration available in the rock core was calculated. **Table 6** shows both the maximum percentage released during the three reactions with pure or impure CO_2 and the percentage released at the end point of the reaction. A higher proportion of both As and U (10 and 1.6%) were released during the impure CO_2SO_2NO reaction than during the pure CO_2 reaction of 1043.70 m. A higher percentage of Pb (9.6%) was also released during the 1043.70 m CO_2SO_2NO reaction, compared to only 2.2% released during the pure CO_2 reaction. However, by the end of the CO_2SO_2NO reaction, the percentage released was lower (relative to the CO_2 reaction) owing to incorporation of Pb in precipitated material or *via* adsorption to Fe-oxide surfaces (**Table 6**). Metals such as Mn and Ba were released in similar proportions in the CO_2 and CO_2SO_2NO reactions of 1043.70 m. These were likely released

TABLE 6 | Selected elements released from the core samples with CO_2 or CO_2SO_2NO reaction, reported as a percentage of the total amount available in the core. The percentages are calculated by mass balance using the maximum released concentration after gas addition and, separately, the concentration at the end of the experiment (denoted "end").

	1043.70 m CO_2	1043.70 m CO_2SO_2NO	1056.03 m CO_2
	Feldspar-rich Ss	Feldspar-rich Ss	Calcite cemented Ss
As	6.7	10.0	1.2
As end	5.9	7.3	0.9
Pb	2.2	9.6	2.0
Pb end	1.9	1.2	0.6
Zn	10.4	6.4	9.5
Zn end	8.4	6.1	9.5
Mn	16.0	15.1	14.0
Mn end	16.0	15.1	14.0
U	1.2	1.6	1.1
U end	1.2	1.3	1.1
Rb	0.8	0.7	0.5
Rb end	0.8	0.7	0.5
Ba	1.4	1.5	5.9
Ba end	1.4	1.5	5.9

from calcite dissolution that occurred in both the pure CO_2 and the CO_2SO_2NO reactions. The proportion of total Ba that was mobilized from 1043.70 m with CO_2 or CO_2SO_2NO was low at 1.4 and 1.5%, respectively (**Table 6**). This reflects the high total Ba concentration in the core, where the majority was hosted in barite. Since barite is a relatively insoluble mineral that did not react, the low mobilized Ba % represents the portion hosted in calcite. This is consistent with the correlation of mobilized Ca with Ba (and Mn) from primarily calcite dissolution (**Supplementary Material**). The proportions of the metals released were generally low, with 14–16% of the total Mn present in the cores mobilized (**Table 6**). This demonstrates that the total metal content of a core is not a good indicator for metal mobilization; rather, CO_2 reaction experiments at reservoir conditions are needed in assessments. In addition, cores with different mineral contents and reactions with different gas mixtures affect the metal mobilization.

A subset of core samples were subject to sequential extractions based on the modified BCF method which has been reported

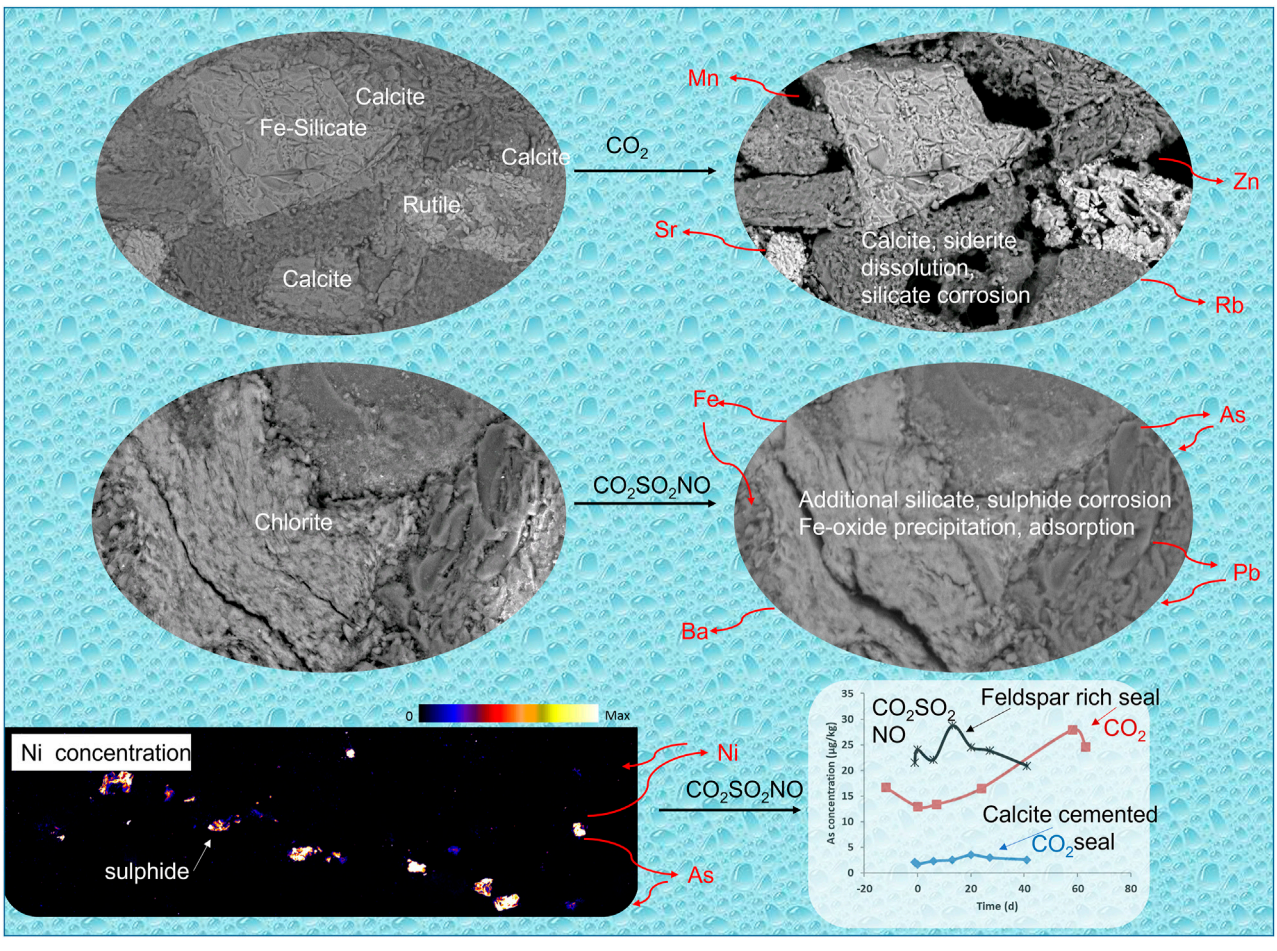

FIGURE 10 | Schematic indicating the key mineral reactions and the associated metal release to water or metal release and subsequent precipitation.

separately (Golding et al., 2019; Kirste et al., 2019; Dawson et al., 2020). Sequential extractions were performed on the two samples from 1043.70 m and 1056.03 m. The water step, weak acid step, and hydroxylamine-hydrochloride at pH 2 step extracted 13, 7, and 26% of the total As from 1043.70 m, respectively. The three steps extracted 6, 18–9, and 27% of the total As from 1056.03 m, respectively (Golding et al., 2019; Kirste et al., 2019; Dawson et al., 2020). This indicated that in both the feldspar-rich sandstone from 1043.70 m and the calcite cemented sandstone, 1056.03 m, As was partially present as a weakly bound species, as well as being extracted from carbonates by weak acid (Golding et al., 2019). The extraction of loosely bound As is consistent with the batch reactions at reservoir conditions where As increased in concentration before addition of the CO_2 or CO_2SO_2NO. The synthetic formation water used in laboratory experiments has small differences with the actual formation water. Therefore ion exchange occurs owing to dis-equilibration of the water and rock core. This initial change before CO_2 addition is a limitation of laboratory experiments in general and does not represent the likely behavior subsurface. Sequential extractions are an extremely useful and less time-intensive technique than CO_2 reaction experiments to assess a wide range of samples. The mobilization of metals from small quantities of carbonates, for example, could be identified. However, the sequential extraction results represent the maximum possible mobilization of metals from the rocks, whereas CO_2 reaction experiments take account of precipitation and other processes that subsequently may immobilize metals. In general, both techniques should be employed, and the combined data should be used for predictive model input and refinement.

The Evergreen Formation studied here is a heterogeneous, but thick, sealing package overlying the Precipice Sandstone reservoir. The Evergreen Formation seal consists of interbedded sandstones, carbonate cemented sandstones, mudstones, and ironstone and has been assessed to be a good regional seal (Farquhar et al., 2015; La Croix et al., 2020a; Pearce et al., 2020). The Precipice Sandstone reservoir is a quartz-rich sandstone with high porosity and permeability and has also been assessed to be a generally suitable storage reservoir (Pearce et al., 2019b). The current study forms a part of a larger assessment, where the Glenhaven site (in the north of the Surat Basin, containing the West Wandoan 1 well) was found to be suitable for a small demonstration-scale CO_2 injection study. The metals mobilized were predicted in reservoir-scale models to be partly re-sequestered, and restricted to the extent of the injected CO_2 plume (Golding et al., 2019). However, regions of the southern and central Surat Basin were deemed to be more suitable for larger industrial-scale CO_2 storage owing to several reasons including the greater storage depths, lower water quality, and greater distance from water bores (Garnett et al., 2019; Pearce et al., 2022b). Although CO_2 injection at the Glenhaven site did not go ahead, the methods and learnings from that site have guided the assessment of the proposed high-prospectivity storage site in the southern Surat Basin.

This study has shown that metals and other environmentally regulated elements including As can be mobilized by CO_2–water–rock reactions during CO_2 geological storage (**Figure 10**). The type and concentrations of metals mobilized depend on the rock mineralogy and the injection gas stream. Even low concentrations of SOx and NOx in the CO_2 stream can affect metal mobilization. Carbonate minerals were the main mobilization sources and are ubiquitous in potential storage reservoirs and seals worldwide. Carbonates may be a source of metals even when present in small amounts, such as grain coatings, that may fall below the detection limit of XRD. Sulfides, apatite, and silicate minerals were additional sources in the current study, especially in the presence of impure CO_2. CO_2 storage sites worldwide should assess the potential risks to water quality in the CO_2 storage complex and overlying formations.

The results here are also relevant to predicting metal mobilization behavior in the unlikely event of a leak into low-salinity aquifers overlying active or target sites of CO_2 storage worldwide. More broadly understanding the impacts of water–rock reactions and metal mobilization on water resources has environmental applications in diverse and developing industries including shale gas, hydrogen storage, enhanced oil recovery, and geothermal energy production (Chermak and Schreiber, 2014; Pearce et al., 2021a; Heinemann et al., 2021; Pearce et al., 2022a) or in processes such as methane leakage (Forde et al., 2019).

This work should be expanded in future to assess metal mobilization from mudstone, evaporite, and shale seal rocks and overlying aquifer core, over a broader range of core mineralogies. The porosity and permeability of caprock seals and the CO_2 reaction–induced changes to the porosity and permeability will have implications for CO_2 and fluid migration (Armitage et al., 2010). Although porosity and permeability were not measured in the current study, dissolution of calcite cement opened intergranular pores in the seal cores after CO_2 and CO_2SO_2NO reaction. Future work should also assess the CO_2 reaction–induced changes to seal rock permeability. In addition, in "hub" style storage sites where a range of CO_2 streams from different sources and with different compositions, are mixed and stored, a range of gas mixtures should be tested in laboratory experiments and experiments upscaled through geochemical models. Future work could also characterize available core that has been exposed to naturally occurring CO_2 (+/- impurity gases) and deep fluids over geological time scales from a variety of Australian aquifers or sites, including in the Surat Basin. This data should be used to understand the long-term behavior of metals and how they are released or re-sequestered into minerals over longer timescales and may be used to validate long-term predictive models.

CONCLUSION

- Evergreen Formation caprock seals from a target CO_2 storage site were characterized. Three samples, an ironstone from the regional seal, a feldspar-rich sandstone seal, and a calcite cemented sandstone seal, were characterized by XFM for metals in specific minerals. Two samples were reacted with pure CO_2 or CO_2 containing SO_2 and NO at reservoir conditions.
- Each metal was generally hosted in several minerals. Although sulfides typically contained the highest metal content,

carbonates were more easily dissolved in the presence of CO_2; therefore, they were often the main sources.
- Calcite dissolution and corrosion of plagioclase, chlorite, kaolinite, illite, and sulfides was observed after pure CO_2 reaction. On impure CO_2 reaction, additionally, apatite, pyrite, and sphalerite cements were corroded or completed dissolved.
- Fe, Pb, As, Ni, Cr, and Cd were generally released in CO_2 rock reactions but were subsequently re-precipitated or adsorbed. Dissolved metals such as Mn, Rb, Ca, Co, and Si generally increased in concentration over the experiment time scales. Mn and Sr were released mainly from calcite dissolution. Plagioclase was a second source of dissolved Sr, and chlorite was a second source of Mn.
- Considering that these caprocks had undergone previous natural alteration or weathering, Mn, Pb, As, Si, etc. had been naturally captured in carbonates, sulfides, and silica cement.
- The rock mineral content and the injected gas mixture had an impact on the type and concentration of metals released. The total metal content of a rock is not a good indicator for metal mobilization; rather, detailed characterization of the metal hosts and experiments with CO_2 and the specific injection gas mixture under reservoir conditions are needed in CO_2 storage site assessments.
- Carbonate minerals are ubiquitous in potential CO_2 storage reservoirs and seals worldwide and were the main sources of metals mobilized in CO_2–water–rock reactions. In impure CO_2 reactions, sulfides, apatite, and silicates were secondary sources. Potential risks to water quality should be assessed in CO_2 storage complexes and overlying aquifers worldwide.

DATA AVAILABILITY STATEMENT

The original contributions presented in the study are included in the article/**Supplementary Material**; further inquiries can be directed to the corresponding author.

AUTHOR CONTRIBUTIONS

JP: conceptualization, methodology, formal analysis, investigation, writing—original draft, visualization, and funding acquisition; GD: formal analysis, validation, investigation, and writing—review and editing; GS: investigation, visualizations, formal analysis, writing—original draft, and funding acquisition; DP: formal analysis, resources, data curation, and writing—review and editing; DK: investigation, formal analysis, and writing—review and editing; SG: writing—review and editing, supervision, funding acquisition, and project administration.

FUNDING

Part of this research was funded by Australian National Low Emissions Coal Research and Development (ANLEC R&D) project 7-0115-0236. ANLEC R&D is supported by Low Emission Technology Australia (LETA) and the Australian Government through the Clean Energy Initiative. Part of this research was undertaken on the XFM beamline at the Australian Synchrotron, part of ANSTO, funded by AS171/XFM/11602 "Sources of element mobilisation to groundwater during carbon dioxide geological storage." We acknowledge travel funding provided by the International Synchrotron Access Program (ISAP) managed by the Australian Synchrotron, part of ANSTO, and funded by the Australian Government.

ACKNOWLEDGMENTS

We acknowledge the facilities, and the scientific and technical assistance, of the Australian Microscopy and Microanalysis Research Facility at the Centre for Microscopy and Microanalysis, The University of Queensland. Two reviewers, along with Richard Worden and Maxim Lebedev, are thanked for their comments that have improved this manuscript.

SUPPLEMENTARY MATERIAL

The Supplementary Material for this article can be found online at: https://www.frontiersin.org/articles/10.3389/fenrg.2022.873813/full#supplementary-material

REFERENCES

Alemu, B. L., Aagaard, P., Munz, I. A., and Skurtveit, E. (2011). Caprock Interaction with CO2: A Laboratory Study of Reactivity of Shale with Supercritical CO2 and Brine. *Appl. Geochem.* 26, 1975–1989. doi:10.1016/j.apgeochem.2011.06.028

Armitage, P. J., Faulkner, D. R., and Worden, R. H. (2013). Caprock Corrosion. *Nat. Geosci.* 6, 79–80. doi:10.1038/ngeo1716

Armitage, P. J., Worden, R. H., Faulkner, D. R., Aplin, A. C., Butcher, A. R., and Iliffe, J. (2010). Diagenetic and Sedimentary Controls on Porosity in Lower Carboniferous Fine-Grained Lithologies, Krechba Field, Algeria: A Petrological Study of a Caprock to a Carbon Capture Site. *Mar. Petroleum Geol.* 27, 1395–1410. doi:10.1016/j.marpetgeo.2010.03.018

Bachu, S., Gunter, W. D., and Perkins, E. H. (1994). Aquifer Disposal of CO2: Hydrodynamic and Mineral Trapping. *Energy Convers. Manag.* 35, 269–279. doi:10.1016/0196-8904(94)90060-4

Barakat, S., Cook, B., D'Amore, K., Diaz, A., and Bracho, A. (2019). An Australian First Initiative to Re-develop the First Commercial Onshore Oilfield into a CO2 Miscible-EOR Project. *APPEA J.* 59, 179–195. doi:10.1071/aj18095

Cahill, A. G., and Jakobsen, R. (2015). Geochemical Modeling of a Sustained Shallow Aquifer CO2 Leakage Field Study and Implications for Leakage and Site Monitoring. *Int. J. Greenh. Gas Control* 37, 127–141. doi:10.1016/j.ijggc.2015.03.011

Cahill, A. G., Jakobsen, R., Mathiesen, T. B., and Jensen, C. K. (2013). Risks Attributable to Water Quality Changes in Shallow Potable Aquifers from Geological Carbon Sequestration Leakage into Sediments of Variable Carbonate Content. *Int. J. Greenh. Gas Control* 19, 117–125. doi:10.1016/j.ijggc.2013.08.018

Carroll, S. A., Keating, E., Mansoor, K., Dai, Z., Sun, Y., Trainor-Guitton, W., et al. (2014). Key Factors for Determining Groundwater Impacts Due to Leakage from Geologic Carbon Sequestration Reservoirs. *Int. J. Greenh. Gas Control* 29, 153–168. doi:10.1016/j.ijggc.2014.07.007

Chermak, J. A., and Schreiber, M. E. (2014). Mineralogy and Trace Element Geochemistry of Gas Shales in the United States: Environmental Implications. *Int. J. Coal Geol.* 126, 32–44. doi:10.1016/j.coal.2013.12.005

Cheung, K., Sanei, H., Klassen, P., Mayer, B., and Goodarzi, F. (2009). Produced Fluids and Shallow Groundwater in Coalbed Methane (CBM) Producing Regions of Alberta, Canada: Trace Element and Rare Earth Element Geochemistry. *Int. J. Coal Geol.* 77, 338–349. doi:10.1016/j.coal.2008.07.012

Choi, B.-Y. (2019). Potential Impact of Leaking CO2 Gas and CO2-rich Fluids on Shallow Groundwater Quality in the Chungcheong Region (South Korea): A Hydrogeochemical Approach. *Int. J. Greenh. Gas Control* 84, 13–28. doi:10.1016/j.ijggc.2019.03.010

CSIRO (2011). *GeoPIXE Software for PIXE and SXRF Imaging*. Available at: http://nmp.csiro.au/GeoPIXE.html (20/4/2016.

Dawson, G., Pearce, J., Kirste, D., and Golding, S. (2020). *A Sequential Extraction Method for Evaluating Rock-Hosted Elements at Conditions Relevant to CO2 Geo-Sequestration, Goldschmidt, Virtual Conference 2020*.

Erdem, M., and Özverdi, A. (2005). Lead Adsorption from Aqueous Solution onto Siderite. *Sep. Purif. Technol.* 42, 259–264. doi:10.1016/j.seppur.2004.08.004

Farquhar, S. M., Pearce, J. K., Dawson, G. K. W., Golab, A., Sommacal, S., Kirste, D., et al. (2015). A Fresh Approach to Investigating CO 2 Storage: Experimental CO 2 -Water-Rock Interactions in a Low-Salinity Reservoir System. *Chem. Geol.* 399, 98–122. doi:10.1016/j.chemgeo.2014.10.006

Feitz, A. J., Ransley, T. R., Dunsmore, R., Kuske, T. J., Hodgkinson, J., Preda, M., et al. (20142009-2011). *Geoscience Australia and Geological Survey of Queensland Surat and Bowen Basins Groundwater Surveys Hydrochemistry Dataset*.

Forde, O. N., Cahill, A. G., Mayer, K. U., Mayer, B., Simister, R. L., Finke, N., et al. (2019). Hydro-biogeochemical Impacts of Fugitive Methane on a Shallow Unconfined Aquifer. *Sci. Total Environ.* 690, 1342–1354. doi:10.1016/j.scitotenv.2019.06.322

Garnett, A., Underschultz, J., and Ashworth, P. (2019). "Scoping Study for Material Carbon Abatement via Carbon Capture and Storage: Project Report," in *The University of Queensland Surat Deep Aquifer Appraisal Project (UQ-SDAAP)* (Brisbane, Australia: The University of Queensland), 392.

Golab, A., Arena, A., Sommacal, S., Goodwin, C., Rajan, P., Dodd, N., et al. (2015). *Milestone 2.9: Final Report of Digital Core Analysis Results for Plug Samples from West Wandoan-1 Well. FEI-Lithicon*. Canberra: Report for ANLEC R&D.

Golding, S. D., Dawson, G. K. W., Pearce, J. K., Farrajota, F., Mernagh, T., Boreham, C. J., et al. (2016). *Authigenic Carbonates in the Great Artesian Basin as Natural Analogues for Mineralisation Trapping*. ANLEC Project 7-1011-0189, CO2CRC report for ANLEC R&D.

Golding, S. D., Pearce, J. K., Dawson, G. K. W., and Kirste, D. M. (2019). *ANLEC Project 7-1115-0236: Mobilisation and Fate of Heavy Metals Released by the GHG Stream*. Report for ANLEC R&D.

Guo, H., Li, Y., Zhao, K., Ren, Y., and Wei, C. (2011). Removal of Arsenite from Water by Synthetic Siderite: Behaviors and Mechanisms. *J. Hazard. Mater.* 186, 1847–1854. doi:10.1016/j.jhazmat.2010.12.078

Guo, H., Stüben, D., and Berner, Z. (2007). Removal of Arsenic from Aqueous Solution by Natural Siderite and Hematite. *Appl. Geochem.* 22, 1039–1051. doi:10.1016/j.apgeochem.2007.01.004

Harkin, T., Filby, I., Sick, H., Manderson, D., and Ashton, R. (2017). Development of a CO2 Specification for a CCS Hub Network. *Energy Procedia* 114, 6708–6720. doi:10.1016/j.egypro.2017.03.1801

Hayes, P., Nicol, C., La Croix, A. D., Pearce, J., Gonzalez, S., Wang, J., et al. (2020). Enhancing Geological and Hydrogeological Understanding of the Precipice Sandstone Aquifer of the Surat Basin, Great Artesian Basin, Australia, through Model Inversion of Managed Aquifer Recharge Datasets. *Hydrogeol. J.* 28, 175–192. doi:10.1007/s10040-019-02079-9

Heinemann, N., Alcalde, J., Miocic, J. M., Hangx, S. J. T., Kallmeyer, J., Ostertag-Henning, C., et al. (2021). Enabling Large-Scale Hydrogen Storage in Porous Media - the Scientific Challenges. *Energy Environ. Sci.* 14, 853–864. doi:10.1039/d0ee03536j

Hodgkinson, J., and Grigorescu, M. (2012). Background Research for Selection of Potential Geostorage Targets-Case Studies from the Surat Basin, Queensland. *Aust. J. Earth Sci.* 60, 71–89. doi:10.1080/08120099.2012.662913

Humez, P., Lions, J., Négrel, P., and Lagneau, V. (2014). CO2 Intrusion in Freshwater Aquifers: Review of Geochemical Tracers and Monitoring Tools, Classical Uses and Innovative Approaches. *Appl. Geochem.* 46, 95–108. doi:10.1016/j.apgeochem.2014.02.008

Jiang, W., Lv, J., Luo, L., Yang, K., Lin, Y., Hu, F., et al. (2013). Arsenate and Cadmium Co-adsorption and Co-precipitation on Goethite. *J. Hazard. Mater.* 262, 55–63. doi:10.1016/j.jhazmat.2013.08.030

Kampman, N., Bertier, P., Busch, A., Snippe, J., Harrington, J., Pipich, V., et al. (2017). Validating Reactive Transport Models of CO2-brine-Rock Reactions in Caprocks Using Observations from a Natural CO2 Reservoir. *Energy Procedia* 114, 4902–4916. doi:10.1016/j.egypro.2017.03.1632

Kampman, N., Busch, A., Bertier, P., Snippe, J., Hangx, S., Pipich, V., et al. (2016). Observational Evidence Confirms Modelling of the Long-Term Integrity of CO2-reservoir Caprocks. *Nat. Commun.* 7, 12268. doi:10.1038/ncomms12268

Karamalidis, A. K., Torres, S. G., Hakala, J. A., Shao, H., Cantrell, K. J., and Carroll, S. (2013). Trace Metal Source Terms in Carbon Sequestration Environments. *Environ. Sci. Technol.* 47, 322–329. doi:10.1021/es304832m

Kharaka, Y. K., Abedini, A. A., Gans, K. D., Thordson, J. J., Beers, S. R., and Thomas, R. B. (2018). Changes in the Chemistry of Groundwater Reacted with CO2: Comparison of Results from Laboratory Experiments and the ZERT Field Site, Bozeman, Montana, USA. *Appl. Geochem.* 98, 75–81. doi:10.1016/j.apgeochem.2018.08.017

Kharaka, Y. K., Cole, D. R., Hovorka, S. D., Gunter, W. D., Knauss, K. G., and Freifeld, B. M. (2006). Gas-water-rock Interactions in Frio Formation Following CO2 Injection: Implications for the Storage of Greenhouse Gases in Sedimentary Basins. *Geol* 34, 577–580. doi:10.1130/g22357.1

Kharaka, Y. K., Thordsen, J. J., Kakouros, E., Ambats, G., Herkelrath, W. N., Beers, S. R., et al. (2010). Changes in the Chemistry of Shallow Groundwater Related to the 2008 Injection of CO2 at the ZERT Field Site, Bozeman, Montana. *Environ. Earth Sci.* 60, 273–284. doi:10.1007/s12665-009-0401-1

Kirsch, K., Navarre-Sitchler, A. K., Wunsch, A., and McCray, J. E. (2014). Metal Release from Sandstones under Experimentally and Numerically Simulated CO2 Leakage Conditions. *Environ. Sci. Technol.* 48, 1436–1442. doi:10.1021/es403077b

Kirste, D., Pearce, J., and Golding, S. (2017). Parameterizing Geochemical Models: Do Kinetics of Calcite Matter? *Procedia Earth Planet. Sci.* 17, 606–609. doi:10.1016/j.proeps.2016.12.162

Kirste, D., Pearce, J. K., Golding, S. D., and Dawson, G. K. W. (2019). Trace Element Mobility during CO2 Storage: Application of Reactive Transport Modelling. *E3S Web Conf.* 98, 04007. doi:10.1051/e3sconf/20199804007

La Croix, A. D., Harfoush, A., Rodger, I., Gonzalez, S., Undershultz, J. R., Hayes, P., et al. (2020a). Reservoir Modelling Notional CO2injection into the Precipice Sandstone and Evergreen Formation in the Surat Basin, Australia. *Pet. Geosci.* 26, 127–140. doi:10.1144/petgeo2019-058

La Croix, A. D., He, J., Bianchi, V., Wang, J., Gonzalez, S., and Undershultz, J. R. (2020b). Early Jurassic Palaeoenvironments in the Surat Basin, Australia - Marine Incursion into Eastern Gondwana. *Sedimentology* 67, 457–485. doi:10.1111/sed.12649

La Croix, A. D., Wang, J., He, J., Hannaford, C., Bianchi, V., Esterle, J., et al. (2019a). Widespread Nearshore and Shallow Marine Deposition within the Lower Jurassic Precipice Sandstone and Evergreen Formation in the Surat Basin, Australia. *Mar. Petroleum Geol.* 109, 760–790. doi:10.1016/j.marpetgeo.2019.06.048

La Croix, A. D., Wang, J., and Underschultz, J. (2019b). "Integrated Facies Analysis of the Precipice Sandstone and Evergreen Formation in the Surat Basin," in *The University of Queensland Surat Deep Aquifer Appraisal Project - Supplementary Detailed Report* (Brisbane: The University of Queensland).

Lawter, A., Qafoku, N. P., Wang, G., Shao, H., and Brown, C. F. (2016). Evaluating Impacts of CO2 Intrusion into an Unconsolidated Aquifer: I. Experimental Data. *Int. J. Greenh. Gas Control* 44, 323–333. doi:10.1016/j.ijggc.2015.07.009

Marcon, V., and Kaszuba, J. P. (2015). Carbon Dioxide-Brine-Rock Interactions in a Carbonate Reservoir Capped by Shale: Experimental Insights Regarding the Evolution of Trace Metals. *Geochimica Cosmochimica Acta* 168, 22–42. doi:10.1016/j.gca.2015.06.037

Maskell, A., Scott, P. M., Buisman, I., and Bickle, M. (2018). A Siltstone Reaction Front Related to CO2- and Sulfur-Bearing Fluids: Integrating Quantitative Elemental Mapping with Reactive Transport Modeling. *Am. Mineralogist* 103, 314–323. doi:10.2138/am-2018-6138ccby

Paterson, D., Jonge, M. D. d., Howard, D. L., Lewis, W., McKinlay, J., Starritt, A., et al. (2011). The X-ray Fluorescence Microscopy Beamline at the Australian Synchrotron. *AIP Conf. Proc.* 1365, 219–222.

Pearce, J., and Dawson, G. (2018). Experimental Determination of Impure CO2 Alteration of Calcite Cemented Cap-Rock, and Long Term Predictions of Cap-Rock Reactivity. *Geosciences* 8, 241. doi:10.3390/geosciences8070241

Pearce, J. K., Brink, F., Dawson, G. W., Poitras, J., Southam, G., Paterson, D. J., et al. (2021a10391). Core Characterisation and Predicted CO2 Reactivity of Sandstones and Mudstones from an Australian Oil Field. *Int. J. Coal Geol.*

Pearce, J. K., Croix, A. D. L., Brink, F., Honari, V., Gonzalez, S., Harfoush, A., et al. (2019a2019). CO2-water-rock Predictions from Aquifer and Oil Field Drill Core Data: The Precipice Sandstone-Evergreen Formation CO2 Storage Reservoir-Seal Pair. *ASEG Ext. Abstr.* 2019, 1–5. doi:10.1080/22020586.2019.12073162

Pearce, J. K., Dawson, G. K. W., Blach, T. P., Bahadur, J., Melnichenko, Y. B., and Golding, S. D. (2018). Impure CO2 Reaction of Feldspar, Clay, and Organic Matter Rich Cap-Rocks: Decreases in the Fraction of Accessible Mesopores Measured by SANS. *Int. J. Coal Geol.* 185, 79–90. doi:10.1016/j.coal.2017.11.011

Pearce, J. K., and Dawson, G. K. W. (2018). "Gas-Water-Mineral Reactivity in Caprocks," in *Geological Carbon Storage*. Editors S. Vialle, J. Ajo-Franklin, and J. W. Carey, 147–165. doi:10.1002/9781119118657.ch7

Pearce, J. K., Dawson, G. K. W., Golab, A., Knuefing, L., Sommacal, S., Rudolph, V., et al. (2019b). A Combined Geochemical and μCT Study on the CO2 Reactivity of Surat Basin Reservoir and Cap-Rock Cores: Porosity Changes, Mineral Dissolution and Fines Migration. *Int. J. Greenh. Gas Control* 80, 10–24. doi:10.1016/j.ijggc.2018.11.010

Pearce, J. K., Dawson, G. K. W., Sommacal, S., and Golding, S. D. (2019c). Experimental and Modelled Reactions of CO2 and SO2 with Core from a Low Salinity Aquifer Overlying a Target CO2 Storage Complex. *Geosciences* 9, 513. doi:10.3390/geosciences9120513

Pearce, J. K., Dawson, G. K. W., Sommacal, S., and Golding, S. D. (2021b). Micro CT and Experimental Study of Carbonate Precipitation from CO2 and Produced Water Co-injection into Sandstone. *Energies* 14, 6998. doi:10.3390/en14216998

Pearce, J. K., Dawson, G. W., Golding, S. D., Southam, G., Paterson, D. J., Brink, F., et al. (2022b). Predicted CO2 Water Rock Reactions in Naturally Altered CO2 Storage Reservoir Sandstones, with Interbedded Cemented and Coaly Mudstone Seals. *Int. J. Coal Geol.* 253, 103966. doi:10.1016/j.coal.2022.103966

Pearce, J. K., Golab, A., Dawson, G. K. W., Knuefing, L., Goodwin, C., and Golding, S. D. (2016). Mineralogical Controls on Porosity and Water Chemistry during O 2 -SO 2 -CO 2 Reaction of CO 2 Storage Reservoir and Cap-Rock Core. *Appl. Geochem.* 75, 152–168. doi:10.1016/j.apgeochem.2016.11.002

Pearce, J. K., Khan, C., Golding, S. D., Rudolph, V., and Underschultz, J. R. (2022c). Geological Storage of CO2 and Acid Gases Dissolved at Surface in Production Water. *J. Petroleum Sci. Eng.* 210, 110052. doi:10.1016/j.petrol.2021.110052

Pearce, J. K., Kirste, D. M., Dawson, G. K. W., Farquhar, S. M., Biddle, D., Golding, S. D., et al. (2015a). SO2 Impurity Impacts on Experimental and Simulated CO2-Water-Reservoir Rock Reactions at Carbon Storage Conditions. *Chem. Geol.* 399, 65–86. doi:10.1016/j.chemgeo.2014.10.028

Pearce, J. K., Kirste, D. M., Dawson, G. K. W., Rudolph, V., and Golding, S. D. (2019d). Geochemical Modelling of Experimental O2–SO2–CO2 Reactions of Reservoir, Cap-Rock, and Overlying Cores. *Appl. Geochem.* 109, 104401. doi:10.1016/j.apgeochem.2019.104400

Pearce, J. K., La Croix, A. D., Brink, F. J., Hayes, P. J., and Underschultz, J. R. (2021c). CO2 Mineral Trapping Comparison in Different Regions: Predicted Geochemical Reactivity of the Precipice Sandstone Reservoir and Overlying Evergreen Formation. *Pet. Geosci.* 27, petgeo2020–106. doi:10.1144/petgeo2020-106

Pearce, J. K., La Croix, A. D., Underschultz, J. R., and Golding, S. D. (2020). Long Term Reactivity of CO2 in a Low Salinity Reservoir-Seal Complex. *Appl. Geochem.* 114, 104529. doi:10.1016/j.apgeochem.2020.104529

Pearce, J. K., Law, A. C. K., Dawson, G. K. W., and Golding, S. D. (2015b). SO2-CO2 and Pure CO2 Reactivity of Ferroan Carbonates at Carbon Storage Conditions. *Chem. Geol.* 411, 112–124. doi:10.1016/j.chemgeo.2015.07.001

Pearce, J., Raza, S., Baublys, K., Hayes, P., Firouzi, M., and Rudolph, V. (2022a). Unconventional CO2 Storage: CO2 Mineral Trapping Predicted in Characterized Shales, Sandstones, and Coal Seam Interburden. *SPE J.*, 1–22. doi:10.2118/209791-pa

Pingitore, N. E., Jr, Lytle, F. W., Davies, B. M., Eastman, M. P., Eller, P. G., and Larson, E. M. (1992). Mode of Incorporation of Sr2+ in Calcite: Determination by X-Ray Absorption Spectroscopy. *Geochimica Cosmochimica Acta* 56, 1531–1538. doi:10.1016/0016-7037(92)90222-5

Porter, R. T. J., Fairweather, M., Pourkashanian, M., and Woolley, R. M. (2015). The Range and Level of Impurities in CO2 Streams from Different Carbon Capture Sources. *Int. J. Greenh. Gas Control* 36, 161–174. doi:10.1016/j.ijggc.2015.02.016

Román-Ross, G., Cuello, G. J., Turrillas, X., Fernández-Martínez, A., and Charlet, L. (2006). Arsenite Sorption and Co-precipitation with Calcite. *Chem. Geol.* 233, 328–336.

Rütters, H., Fischer, S., Hoa, L. Q., Bettge, D., Bäßler, R., Maßmann, J., et al. (2022). Towards Defining Reasonable Minimum Composition Thresholds – Impacts of Variable CO2 Stream Compositions on Transport, Injection and Storage. *Int. J. Greenh. Gas. Control* 114, 103589.

Ryan, C. G., Siddons, D. P., Kirkham, R., Dunn, P. A., Kuczewski, A., Moorhead, G., et al. (2010). The New Maia Detector System: Methods for High Definition Trace Element Imaging of Natural Material. *AIP Conf. Proc.*, 9–17. doi:10.1063/1.3399266

Ryan, C. G., Siddons, D. P., Kirkham, R., Li, Z. Y., de Jonge, M. D., Paterson, D. J., et al. (2014). Maia X-Ray Fluorescence Imaging: Capturing Detail in Complex Natural Samples. *J. Phys. Conf. Ser.* 499, 012002. doi:10.1088/1742-6596/499/1/012002

Shao, H., Freiburg, J. T., Berger, P. M., Taylor, A. H., Cohen, H. F., and Locke, R. A. (2020). Mobilization of Trace Metals from Caprock and Formation Rocks at the Illinois Basin - Decatur Project Demonstration Site under Geological Carbon Dioxide Sequestration Conditions. *Chem. Geol.* 550, 119758. doi:10.1016/j.chemgeo.2020.119758

Shao, H., Kukkadapu, R. K., Krogstad, E. J., Newburn, M. K., and Cantrell, K. J. (2014). Mobilization of Metals from Eau Claire Siltstone and the Impact of Oxygen under Geological Carbon Dioxide Sequestration Conditions. *Geochimica Cosmochimica Acta* 141, 62–82. doi:10.1016/j.gca.2014.06.011

Suckow, A., Raiber, M., Deslandes, A., and Gerber, C. (2018). *Constraining Conceptual Groundwater Models for the Hutton and Precipice Aquifers in the Surat Basin through Tracer Data Final Report*. Australia: CSIRO.

Talman, S. (2015). Subsurface Geochemical Fate and Effects of Impurities Contained in a CO2 Stream Injected into a Deep Saline Aquifer: What Is Known. *Int. J. Greenh. Gas Control* 40, 267–291. doi:10.1016/j.ijggc.2015.04.019

Tsuji, T., Sorai, M., Shiga, M., Fujikawa, S., and Kunitake, T. (2021). Geological Storage of CO 2 -N 2 -O 2 Mixtures Produced by Membrane-based Direct Air Capture (DAC). *Greenh. Gas. Sci. Technol.* 11, 610–618. doi:10.1002/ghg.2099

Turner, L. G., Pearce, J. K., Golding, S. D., Myers, G. A., and Morgan, Q. (2016). *Experiments and Geochemical Simulations of Co-injection of CO2*. SO2 and NO.

Viswanathan, H., Dai, Z., Lopano, C., Keating, E., Hakala, J. A., Scheckel, K. G., et al. (2012). Developing a Robust Geochemical and Reactive Transport Model to Evaluate Possible Sources of Arsenic at the CO2 Sequestration Natural Analog Site in Chimayo, New Mexico. *Int. J. Greenh. Gas Control* 10, 199–214. doi:10.1016/j.ijggc.2012.06.007

Wang, G., Qafoku, N. P., Lawter, A. R., Bowden, M., Harvey, O., Sullivan, C., et al. (2016). Geochemical Impacts of Leaking CO2 from Subsurface Storage Reservoirs to an Unconfined Oxidizing Carbonate Aquifer. *Int. J. Greenh. Gas Control* 44, 310–322. doi:10.1016/j.ijggc.2015.07.002

Wigley, M., Dubacq, B., Kampman, N., and Bickle, M. (2013). Controls of Sluggish, CO2-promoted, Hematite and K-Feldspar Dissolution Kinetics in Sandstones. *Earth Planet. Sci. Lett.* 362, 76–87. doi:10.1016/j.epsl.2012.11.045

Wigley, M., Kampman, N., Dubacq, B., and Bickle, M. (2012). Fluid-mineral Reactions and Trace Metal Mobilization in an Exhumed Natural CO2 Reservoir, Green River, Utah. *Geology* 40, 555–558. doi:10.1130/g32946.1

Wunsch, A., Navarre-Sitchler, A. K., Moore, J., and McCray, J. E. (2014). Metal Release from Limestones at High Partial-Pressures of CO2. *Chem. Geol.* 363, 40–55. doi:10.1016/j.chemgeo.2013.10.036

Wunsch, A., Navarre-Sitchler, A. K., Moore, J., Ricko, A., and McCray, J. E. (2013). Metal Release from Dolomites at High Partial-Pressures of CO2. *Appl. Geochem.* 38, 33–47. doi:10.1016/j.apgeochem.2013.08.005

Yang, C., Mickler, P. J., Reedy, R., Scanlon, B. R., Romanak, K. D., Nicot, J.-P., et al. (2013). Single-well Push-Pull Test for Assessing Potential Impacts of CO2 Leakage on Groundwater Quality in a Shallow Gulf Coast Aquifer in

Cranfield, Mississippi. *Int. J. Greenh. Gas Control* 18, 375–387. doi:10.1016/j.ijggc.2012.12.030

Zheng, L., Apps, J. A., Zhang, Y., Xu, T., and Birkholzer, J. T. (2009). On Mobilization of Lead and Arsenic in Groundwater in Response to CO2 Leakage from Deep Geological Storage. *Chem. Geol.* 268, 281–297. doi:10.1016/j.chemgeo.2009.09.007

Zheng, L., Qafoku, N. P., Lawter, A., Wang, G., Shao, H., and Brown, C. F. (2016). Evaluating Impacts of CO2 Intrusion into an Unconsolidated Aquifer: II. Modeling Results. *Int. J. Greenh. Gas Control* 44, 300–309. doi:10.1016/j.ijggc.2015.07.001

Conflict of Interest: The authors declare that the research was conducted in the absence of any commercial or financial relationships that could be construed as a potential conflict of interest.

Publisher's Note: All claims expressed in this article are solely those of the authors and do not necessarily represent those of their affiliated organizations, or those of the publisher, the editors, and the reviewers. Any product that may be evaluated in this article, or claim that may be made by its manufacturer, is not guaranteed or endorsed by the publisher.